

International Journal of Modern Physics A
 © World Scientific Publishing Company

The XYZ states revisited

Chang-Zheng Yuan

¹ *Institute of High Energy Physics, Chinese Academy of Sciences,
 19B Yuquan Road, Beijing 100049, China*
² *University of Chinese Academy of Sciences,
 19A Yuquan Road, Beijing 100049, China*
yuan cz@ihep.ac.cn

The BESIII and the LHCb became the leading experiments in the study of the exotic states after the Belle and BaBar experiments finished their data taking in the first decade of this century. We review the progress in the study of the XYZ states at BESIII and LHCb experiments with their unique data samples in e^+e^- annihilation at center-of-mass energies of 3.8–4.6 GeV and in pp collision at center-of-mass energies 7, 8, and 13 TeV, respectively. With these data samples, we have deepened our understanding of the most famous charmonium-like states $X(3872)$, $Y(4260)$, $Z_c(3900)$, and $Z_c(4430)$, as well as other similar states like the $Y(4140)$ and $X(3823)$. We review the progress in the study of these states, and also discuss perspectives at future experiments.

Keywords: Exotic states; Hadron spectroscopy; QCD.

PACS numbers: 14.40.Rt, 14.40.Pq, 13.25.Gv, 13.20.Gd, 13.66.Bc

Contents

1. Introduction	2
2. The BESIII and LHCb experiments and data samples	3
2.1. The BESIII experiment	3
2.2. The LHCb experiment	5
3. The iso-triplet charmonium-like states: Z_c s	6
3.1. The $Z_c(3900)$	7
3.1.1. Observation of the $Z_c(3900)$	7
3.1.2. Observation of $Z_c(3900) \rightarrow D\bar{D}^* + c.c.$	8
3.1.3. The quantum numbers	10
3.1.4. Evidence for $Z_c(3900) \rightarrow \rho\eta_c$	11
3.1.5. Hint for $Z_c(3900) \rightarrow \pi h_c$	13
3.1.6. Summary on the $Z_c(3900)$	14

2 *Chang-Zheng Yuan*

3.2.	The $Z_c(4020)$	14
3.2.1.	Observation of the $Z_c(4020)$	14
3.2.2.	Observation of $Z_c(4020) \rightarrow D^* \bar{D}^*$	16
3.2.3.	Search for $Z_c(4020) \rightarrow \pi J/\psi$	17
3.2.4.	Search for $Z_c(4020) \rightarrow \rho \eta_c$	17
3.2.5.	Summary on the $Z_c(4020)$	17
3.3.	The Z_c structures in $\pi\psi(2S)$ system	18
3.3.1.	The $Z_c(4430)$	18
3.3.2.	The Z_c structure in $e^+e^- \rightarrow \pi^+\pi^-\psi(2S)$	20
3.4.	Summary on the Z_c states	21
4.	The $X(3872)$	22
4.1.	The spin-parity of the $X(3872)$	22
4.2.	The puzzling radiative transitions $X(3872) \rightarrow \gamma J/\psi$ and $\gamma\psi(2S)$	23
4.3.	Decay branching fractions of the $X(3872)$	24
4.4.	Observation of $e^+e^- \rightarrow \gamma X(3872)$	25
4.5.	More studies at BESIII and LHCb?	26
5.	The Y s: vector structures in e^+e^- annihilation	27
5.1.	$e^+e^- \rightarrow \pi^+\pi^- J/\psi$	27
5.2.	$e^+e^- \rightarrow \pi^+\pi^- h_c$	28
5.3.	$e^+e^- \rightarrow \pi^+\pi^-\psi(2S)$	29
5.4.	$e^+e^- \rightarrow D^0 D^{*-} \pi^+ + c.c.$	31
5.5.	$e^+e^- \rightarrow \omega \chi_{cJ}$ and $\phi \chi_{cJ}$	32
5.6.	$e^+e^- \rightarrow \eta h_c$	34
5.7.	$e^+e^- \rightarrow \eta J/\psi$ and $\eta' J/\psi$	34
5.8.	Efforts in extracting resonant parameters from combined fits	36
6.	Observation of $\psi(1^3D_2)$	37
7.	The $Y(4140)$ and other states in $\phi J/\psi$ system	38
8.	Summary and Perspectives	39

1. Introduction

In the conventional quark model, mesons are composed of one quark and one anti-quark, while baryons are composed of three quarks. Although this picture is very simple, it describes almost all the hadrons observed so far.¹ However, exotic hadronic states with other configurations have been proposed and searched for since long time ago.²

Many charmonium and charmonium-like states were discovered at two B -factories BaBar³ and Belle⁴ in the first decade of this century.⁵ Whereas some of these are good candidates of charmonium states, as predicted in different models, many other states have exotic properties, which may indicate that exotic states, such as multi-quark state, meson molecule, hybrid, or hadron-quarkonium, have been observed.⁶ Experimentally, these states are also called XYZ states, to indicate their nature is still unclear.

BaBar³ and Belle⁴ experiments finished their data taking in 2008 and 2010 with total integrated luminosity of 557 and 1040 fb⁻¹, respectively. The data are still used for various physics analyses until now. In 2008, two new experiments, the BESIII,⁷ a τ -charm factory experiment at the BEPCII e^+e^- collider, and the LHCb,⁸ a B -factory experiment at the LHC, started data taking, and contributed to the study of the XYZ particles ever since.

In this article, we review the study of the XYZ particles from the BESIII⁷ and the LHCb⁸ experiments. We first introduce the two experiments, the data samples, and the advantages and disadvantages for the study of the hadron spectroscopy at these experiments, and then focus on the measurements of the three mostly studied XYZ states, i.e., the $X(3872)$, the $Y(4260)$, and the $Z_c(3900)$. We also discuss other XYZ states, including the $Z_c(4020)$, the $Z_c(4430)$, the $X(3823)$, and the $Y(4140)$ family. At the end of the article, we give perspectives on the study at these two experiments, and also point out possible studies at next generation experiments.

2. The BESIII and LHCb experiments and data samples

2.1. The BESIII experiment

The BESIII experiment⁷ at the BEPCII storage ring started its first collisions in the tau-charm energy region in 2008. The BESIII detector has an effective geometrical acceptance of 93% of 4π . It contains a small cell helium-based multi-layered drift chamber (MDC) which provides momentum measurements of charged particles; a time-of-flight system (TOF) based on plastic scintillator which helps to identify charged particles; an electromagnetic calorimeter (EMC) made of CsI(Tl) crystals which is used to measure the energies of photons and provide trigger signals; and a muon system (MUC) made of Resistive Plate Chambers (RPC). The momentum resolution of the charged particles is 0.5% at 1 GeV/ c in a 1 Tesla magnetic field; the energy loss (dE/dx) measurement provided by the MDC has a resolution better than 6% for electrons from Bhabha scattering; the photon energy resolution can reach 2.5% (5%) at 1 GeV in the barrel (endcaps) of the EMC; and the time resolution of TOF is 80 ps in the barrel and 110 ps in the endcaps. In 2015, the endcap TOF was replaced with MRPC, and the time resolution is improved to be 60 ps.⁹

After a few years running at energies for its well-defined physics programs,¹⁰ i.e., at J/ψ and $\psi(2S)$ peaks in 2009 and the $\psi(3770)$ peak in 2010 and 2011, the BESIII experiment started to collect data for the study of the XYZ particles, which

were not described in the Yellow Book.¹⁰ BESIII took its first data sample at the $\psi(4040)$ resonance in May 2011, with the aim of searching for the $X(3872)$ and the excited P -wave charmonium spin-triplet states in the $\psi(4040)$ radiative transitions. This sample is about 0.5 fb^{-1} , which is limited by the one-month running time left after the $\psi(3770)$ data taking in the 2010–2011 run.

The upgrade of BEPCII’s LINAC in summer 2012 increased the highest beam energy from 2.1 to 2.3 GeV, making it possible to collect data at higher center-of-mass (c.m.) energies (up to 4.6 GeV). In one month’s data of 525 pb^{-1} (from December 14, 2012 to January 14, 2013) at c.m. energy of 4.26 GeV, the charged charmonium-like state $Z_c(3900)$ was discovered,¹¹ this results in changes to the data collection plan for the 2012–2013 run. More data were accumulated at c.m. energies of 4.26 GeV and then 4.23 GeV where a higher $e^+e^- \rightarrow \pi^+\pi^- J/\psi$ production rate is observed. Data at the $Y(4360)$ peak were also obtained in spring 2013, and data at even higher energies (4.42 and 4.6 GeV) were recorded in 2014 after a fine scan of the total hadronic cross sections between 3.8 and 4.6 GeV at more than 100 energy points (“ R -scan data” hereafter), with a total integrated luminosity of about 800 pb^{-1} . The data taking in 2015–2016 was dedicated to D_s decays at c.m. energy $\sqrt{s} = 4.178 \text{ GeV}$ which can also be used for XYZ study, followed by more data points between 4.19 and 4.28 GeV dedicated to XYZ related analyses in 2016–2017 running year.

The data samples for the XYZ study (“XYZ data” hereafter) are presented in Table 1, which lists the nominal c.m. energy, measured c.m. energy (when it is available), and integrated luminosity at each energy point. These data were used for all the analyses presented in this article. The c.m. energy and the luminosity of the R -scan data can be found in Ref. 14 and are not listed here.

Compared with the B factories BaBar and Belle, BESIII has its advantages in the study of the XYZ states, especially in the study of the vector Y states. BESIII collects e^+e^- annihilation data at c.m. energies correspond to the production of the Y states directly, while the B factories use data produced via initial state radiation (ISR), so the BESIII has a much higher detection efficiency and can take more data at any energy of interest (for example, the efficiency is 46% at BESIII¹¹ and about 10% at Belle¹⁵ for selecting $Y(4260) \rightarrow \pi^+\pi^- J/\psi \rightarrow \pi^+\pi^-\ell^+\ell^-$ ($\ell = e, \text{ or } \mu$) events). This makes the study of the Z_c states from the Y decays also more efficient at BESIII than at the B factories. However, B factories can measure the cross sections in a wide energy range since all the events are produced at the same time, while BESIII needs to tune the c.m. energy point by point to collect data, thus can only cover limited energy range.

Needless to say that the B factories can study the XYZ states with B decays, two-photon fusion, as well as double-charmonium production and $\Upsilon(nS)$ ($n = 1, 2, 3$) decays, while BESIII is limited to e^+e^- annihilation.

Table 1. The measured c.m. energy,¹² integrated luminosity¹³ of each data sample collected for the study of the XYZ states. The uncertainties on the integrated luminosities are statistical only; a 1% systematic uncertainty common to all the data points is not listed. “_” means not available yet and numbers without error are rough estimation.

Data sample	c.m. energy (MeV)	\mathcal{L} (pb ⁻¹)
3810	3807.65±0.10±0.58	50.54±0.03
3900	3896.24±0.11±0.72	52.61±0.03
4009	4007.62±0.05±0.66	481.96±0.01
4090	4085.45±0.14±0.66	52.63±0.03
4180	4178	~ 3190
4190	4188.59±0.15±0.68	43.09±0.03
4190	–	~ 500
4200	–	~ 500
4210	4207.73±0.14±0.61	54.55±0.03
4210	–	~ 500
4220	4217.13±0.14±0.67	54.13±0.03
4220	–	~ 500
4230	4226.26±0.04±0.65	1091.74±0.15
4237	–	~ 500
4245	4241.66±0.12±0.73	55.59±0.04
4246	–	~ 500
4260	4257.97±0.04±0.66	825.67±0.13
4270	–	~ 500
4280	–	~ 200
4310	4307.89±0.17±0.63	44.90±0.03
4360	4358.26±0.05±0.62	539.84±0.10
4390	4387.40±0.17±0.65	55.18±0.04
4420	4415.58±0.04±0.72	1073.56±0.14
4470	4467.06±0.11±0.73	109.94±0.04
4530	4527.14±0.11±0.72	109.98±0.04
4575	4574.50±0.18±0.70	47.67±0.03
4600	4599.53±0.07±0.74	566.93±0.11

2.2. The LHCb experiment

LHCb is a dedicated heavy flavor physics experiment at the LHC but has unexpected potential in the study of hadron spectroscopy. The detector is a single-arm spectrometer with a forward angular coverage from approximately 15 mrad to 300 (250) mrad in the bending (non-bending) plane.⁸

The spectrometer magnet is a warm dipole magnet providing an integrated field of about 4 Tm, which deflects charged particles in the horizontal plane. The tracking system consists of the VERtEX LOcator (VELO), and four planar tracking stations: the Tracker Turicensis (TT) upstream of the dipole magnet, and tracking stations T1–T3 downstream of the magnet. Charged particles require a minimum momentum of 1.5 GeV/*c* to reach the tracking stations, T1–T3. Charged hadron identification in the momentum range from 2 to 100 GeV/*c* is achieved by two

6 *Chang-Zheng Yuan*

Ring Imaging Cherenkov detectors (RICH1 and RICH2). The calorimeter system is composed of a Scintillating Pad Detector (SPD), a Preshower (PS), a shashlik type electromagnetic calorimeter (ECAL) and a hadronic calorimeter (HCAL). The muon detection system provides muon identification and contributes to the L0 trigger of the experiment. The minimum momentum that a muon must have to traverse the five stations is approximately 6 GeV/ c .

The integrated luminosity recorded by the LHCb detector is 1.1 fb⁻¹ at 7 TeV in 2011, 2.1 fb⁻¹ at 8 TeV in 2012, and about 4 fb⁻¹ at 13 TeV from 2015 up to now, and the plan is to accumulate up to 5 fb⁻¹ at 13 TeV by the end of 2018.¹⁶

Due to the large production cross sections, more B mesons and other particles are produced at LHCb than at other experiments like BaBar and Belle. However, to avoid background from direct pp collision, many of the studies were performed with a mother particle which has a long decay length. So far, most of the results related to the XYZ particles are from B decays. The large B sample makes the determination of the quantum numbers and the decay dynamics of the XYZ states possible via partial wave analysis (PWA) of the B decays.

3. The iso-triplet charmonium-like states: Z_c s

Searching for the charged charmonium-like state is one of the most promising ways of studying the exotic hadrons, since such a state must contain at least four quarks and thus could not be a conventional meson. The searches were performed in the combination of one charged pion and a charmonium state, like J/ψ , $\psi(2S)$, and h_c , since they are narrow and the reconstruction in the experiment is relatively easy.

The first reported charged charmonium-like state, $Z_c(4430)^-$, was in the $\pi^-\psi(2S)$ invariant mass distribution in $B \rightarrow K\pi^-\psi(2S)$ decays in the Belle experiment,^{17,18} it was confirmed by the LHCb experiment seven years later.¹⁹ The $Z_c(3900)^-$ was observed in π^-J/ψ invariant mass distribution in the study of $e^+e^- \rightarrow \pi^+\pi^-J/\psi$ at BESIII¹¹ and Belle²⁰ experiments, and the $Z_c(4020)^-$ was observed in π^-h_c system in $e^+e^- \rightarrow \pi^+\pi^-h_c$ ²¹ only at BESIII. There is also evidence for Z_c structures in the $\pi\psi(2S)$ system at Belle²² and BESIII²³ in $e^+e^- \rightarrow \pi^+\pi^-\psi(2S)$.

These states seem to indicate that a new class of hadrons has been observed. As there are at least four quarks within all these Z_c states, they have been interpreted either as compact tetraquark states, molecular states of two charmed mesons ($\bar{D}D^* + c.c.$, \bar{D}^*D^* , $\bar{D}D_1 + c.c.$, $\bar{D}^*D_1 + c.c.$, etc.), hadro-quarkonium states, or other configurations.⁶

There are other Z_c states observed in different processes, such as the two structures at masses 4050 and 4250 MeV/ c^2 in $\pi^-\chi_{c1}$ system in $B \rightarrow K\pi^-\chi_{c1}$ decays;²⁴ and the $Z_c(4200)^-$ in the π^-J/ψ invariant mass distribution in $B \rightarrow K\pi^-J/\psi$ decays²⁵ from Belle experiment. We will focus on the $Z_c(4430)^-$, $Z_c(3900)^-$, and

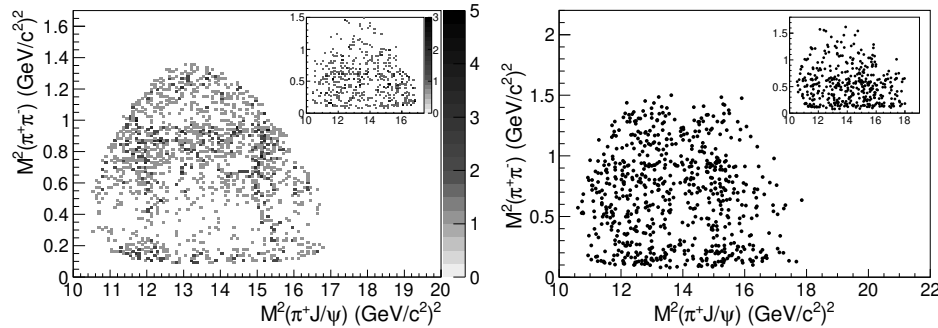


Fig. 1. Dalitz plots for selected $e^+e^- \rightarrow \pi^+\pi^-J/\psi$ events in the J/ψ signal region at BESIII (left panel) and at Belle (right panel). The insets show background events from the J/ψ mass sidebands (not normalized).

$Z_c(4020)^-$ in this article as new information is available recently, we also report new observation in $\pi^-\psi(2S)$ system from BESIII experiment.²³

3.1. The $Z_c(3900)$

3.1.1. Observation of the $Z_c(3900)$

The BESIII experiment studied the $e^+e^- \rightarrow \pi^+\pi^-J/\psi$ process at a c.m. energy of 4.26 GeV using a 525 pb^{-1} data sample,¹¹ with J/ψ decays into a pair of e^+e^- or $\mu^+\mu^-$. 595 ± 28 signal events in the e^+e^- mode and 882 ± 33 signal events in the $\mu^+\mu^-$ mode are reconstructed and the cross section is measured to be $(62.9 \pm 1.9 \pm 3.7) \text{ pb}$, which agrees with the existing results from the BaBar²⁶ and Belle¹⁵ experiments. The J/ψ signal is selected by requiring the invariant mass of the lepton pair is consistent with the J/ψ , and a sample of 1595 $\pi^+\pi^-J/\psi$ events with a purity of 90% is obtained. The intermediate states are studied by examining the Dalitz plot (shown in Fig. 1) of the selected candidate events.

Besides the known σ and $f_0(980)$ structures in the $\pi^+\pi^-$ system, a structure at around $3.9 \text{ GeV}/c^2$ was observed in the $\pi^\pm J/\psi$ invariant mass distribution with a statistical significance larger than 8σ , which is referred to as the $Z_c(3900)$. A fit to the $\pi^\pm J/\psi$ invariant mass spectrum with a constant width Breit-Wigner (BW) function (see Fig. 2), neglecting interference with other amplitudes, results in a mass of $(3899.0 \pm 3.6 \pm 4.9) \text{ MeV}/c^2$ and a width of $(46 \pm 10 \pm 20) \text{ MeV}$. The associated production ratio is measured to be $\frac{\sigma(e^+e^- \rightarrow \pi^\pm Z_c(3900)^\mp \rightarrow \pi^+\pi^-J/\psi)}{\sigma(e^+e^- \rightarrow \pi^+\pi^-J/\psi)} = (21.5 \pm 3.3 \pm 7.5)\%$.

At the Belle experiment, the cross section of $e^+e^- \rightarrow \pi^+\pi^-J/\psi$ is measured from 3.8–5.5 GeV using the ISR method with a 967 fb^{-1} data sample collected at or near the $\Upsilon(nS)$ ($n = 1, 2, 4, 5$) resonances.²⁰ Events in the $Y(4260)$ signal region ($4.15 < M(\pi^+\pi^-J/\psi) < 4.45 \text{ GeV}/c^2$) are investigated, as is shown in

8 Chang-Zheng Yuan

Fig. 1. The $Z_c(3900)$ state (referred to as $Z(3900)^+$ in the Belle paper) with a mass of $(3894.5 \pm 6.6 \pm 4.5)$ MeV/ c^2 and a width of $(63 \pm 24 \pm 26)$ MeV is observed in the $\pi^\pm J/\psi$ mass spectrum (see Fig. 2) with a statistical significance larger than 5.2σ . The ratio of the production rates $\frac{\sigma(e^+e^- \rightarrow \pi^\pm Z_c(3900)^\mp \rightarrow \pi^\pm \pi^\mp J/\psi)}{\sigma(e^+e^- \rightarrow \pi^+ \pi^- J/\psi)} = (29.0 \pm 8.9)\%$, where the error is statistical only.

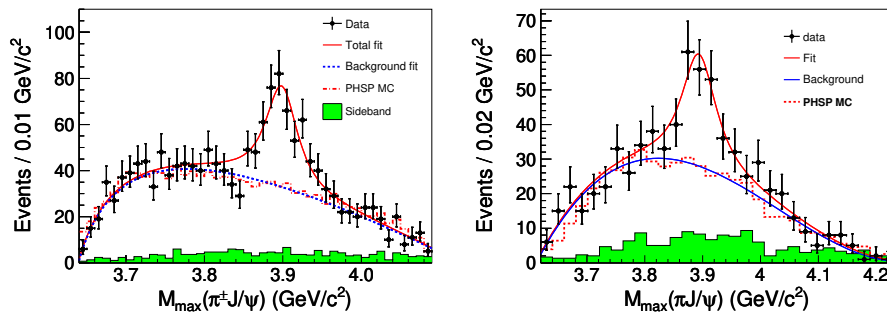


Fig. 2. Unbinned maximum likelihood fit to the distribution of the $M_{\max}(\pi J/\psi)$ (left panel from BESIII and right panel from Belle). Points with error bars are data, the curves are the best fit, the dashed histograms are the phase space distributions and the shaded histograms are the non- $\pi^+ \pi^- J/\psi$ background estimated from the normalized J/ψ sidebands.

The $Z_c(3900)$ state was confirmed shortly after with CLEO-c data at a c.m. energy of 4.17 GeV,²⁷ and the mass and width agreed very well with the BESIII and Belle measurements. In addition, a 3.5σ evidence for $Z_c(3900)^0$ in the CLEO-c data was also reported in $e^+e^- \rightarrow \pi^0 \pi^0 J/\psi$ process.²⁷

BESIII measured the cross sections of $e^+e^- \rightarrow \pi^0 \pi^0 J/\psi$ with data at c.m. energy ranges from 4.19–4.42 GeV.²⁸ A neutral state $Z_c(3900)^0 \rightarrow \pi^0 J/\psi$ with a significance of 10.4σ was observed, with the mass and width measured to be $(3894.8 \pm 2.3 \pm 3.2)$ MeV/ c^2 and $(29.6 \pm 8.2 \pm 8.2)$ MeV, respectively. This state decays to $\pi^0 J/\psi$ and its mass is close to that of $Z_c(3900)^\pm$, so it is interpreted as the neutral partner of the $Z_c(3900)^\pm$. The measured production rate of $e^+e^- \rightarrow \pi^0 Z_c(3900)^0$ is about half of that for $e^+e^- \rightarrow \pi^+ Z_c(3900)^- + c.c.$, which is consistent with the isospin symmetry expectation. This determines the $Z_c(3900)$ is an isovector state.

3.1.2. Observation of $Z_c(3900) \rightarrow D\bar{D}^* + c.c.$

The $Z_c(3900)$ observed in the $\pi J/\psi$ final state is close to and above the $D\bar{D}^* + c.c.$ mass threshold. With the same data sample at $\sqrt{s} = 4.26$ GeV, the BESIII experiment studied $e^+e^- \rightarrow \pi^\pm (D\bar{D}^*)^\mp$ and observed the open-charm decay $Z_c(3900)^\pm \rightarrow (D\bar{D}^* + c.c.)^\pm$.²⁹

The $e^+e^- \rightarrow \pi^+ (D\bar{D}^*)^- + c.c.$ events are selected by a so-called single-tag technique in which only the bachelor π^\pm and one final-state D meson are detected,

and the \bar{D}^* is inferred from energy-momentum conservation. In this analysis, both isospin channels $\pi^+ D^0 D^{*-} + c.c.$ and $\pi^+ D^- D^{*0} + c.c.$ are studied. The D mesons are reconstructed in the $D^0 \rightarrow K^- \pi^+$ and $D^+ \rightarrow K^- \pi^+ \pi^+$ decay channels.

A structure close to the threshold is observed in the $(D\bar{D}^*)^\pm$ invariant mass distribution. When fitted to a BW function with mass-dependent width, the pole mass and width are determined to be $(3883.9 \pm 1.5 \pm 4.2)$ MeV/ c^2 and $(24.8 \pm 3.3 \pm 11.0)$ MeV, respectively (see Fig. 3). The production rate is measured to be $\sigma(e^+e^- \rightarrow \pi^\mp Z_c(3900)^\pm) \times \mathcal{B}(Z_c(3900)^\pm \rightarrow (D\bar{D}^*)^\pm) = (83.5 \pm 6.6 \pm 22.0)$ pb.

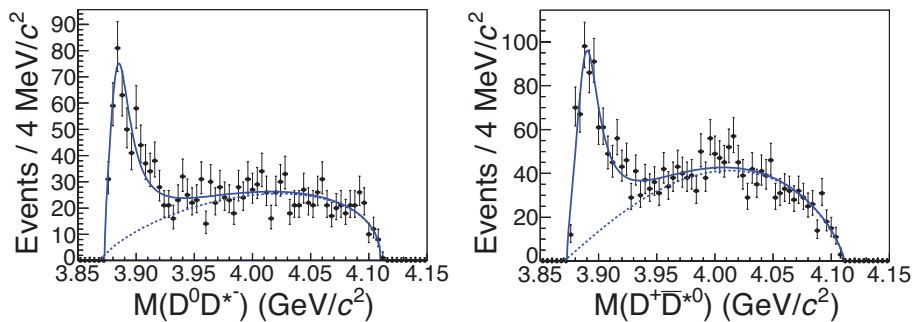


Fig. 3. The $M(D^0 D^{*-})$ (left) and $M(D^+ \bar{D}^{*0})$ (right) distributions for selected events at $\sqrt{s} = 4.26$ GeV in the single-tag analysis. The curves show the best fits.

The analysis is refined with double-tag method and more luminosity.³⁰ In this analysis, both $e^+e^- \rightarrow \pi^+ D^0 D^{*-} + c.c.$ and $\pi^+ D^- D^{*0} + c.c.$ are measured with data samples at $\sqrt{s}=4.23$ and 4.26 GeV. The bachelor π^+ and the D meson pair in the final state are reconstructed, with the π from D^{*-} and D^{*0} decays inferred using energy-momentum conservation. The D^0 is reconstructed in four decay modes ($K^- \pi^+$, $K^- \pi^+ \pi^0$, $K^- \pi^+ \pi^+ \pi^-$, and $K^- \pi^+ \pi^+ \pi^- \pi^0$), and the D^- in six decay modes ($K^+ \pi^- \pi^-$, $K^+ \pi^- \pi^- \pi^0$, $K_S^0 \pi^-$, $K_S^0 \pi^- \pi^0$, $K_S^0 \pi^+ \pi^- \pi^-$, and $K^+ K^- \pi^-$). The double D tag technique allows the use of more D decay modes and the background level is greatly suppressed.

The $M(D\bar{D}^*)$ distributions for the two processes at $\sqrt{s}=4.23$ and 4.26 GeV are fitted simultaneously (shown in Fig. 4) with a BW function for the $Z_c(3900)$ signal and a phase space distribution for the background, added incoherently. The mass and width of $Z_c(3900)$ are fitted to be (3890.3 ± 0.8) MeV/ c^2 and (31.5 ± 3.3) MeV, respectively, correspond to the pole mass and pole width of $(3881.7 \pm 1.6 \pm 1.6)$ MeV/ c^2 and $(26.6 \pm 2.0 \pm 2.1)$ MeV, respectively.

The production rate is measured as $\sigma(e^+e^- \rightarrow \pi^\mp Z_c(3900)^\pm) \times \mathcal{B}(Z_c(3900)^\pm \rightarrow (D\bar{D}^*)^\pm) = (141.6 \pm 7.9 \pm 12.3)$ pb at $\sqrt{s}=4.23$ GeV, and $(108.4 \pm 6.9 \pm 8.8)$ pb at $\sqrt{s}=4.26$ GeV.

The pole position of the $Z_c(3900)$ and the production rate are consistent with but more precise than those from single-tag analysis. The double-tag analysis only

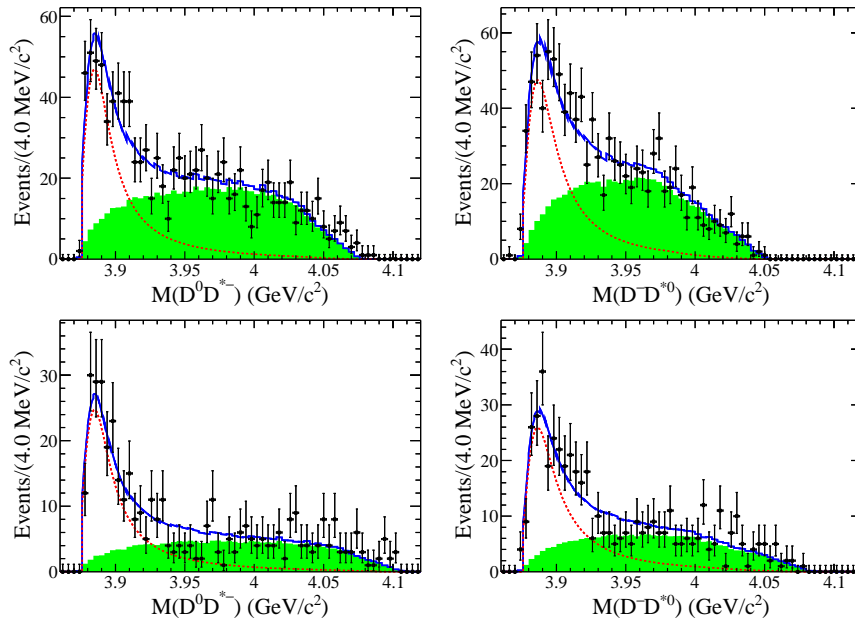


Fig. 4. Simultaneous fits to the $M(D\bar{D}^*)$ distributions in the double-tag analysis. The top row is from data at $\sqrt{s}=4.23$ GeV and the bottom row at $\sqrt{s}=4.26$ GeV. The left column is for $e^+e^- \rightarrow \pi^+ D^0 D^{*-} + c.c.$ and the right column for $e^+e^- \rightarrow \pi^+ D^- D^{*0} + c.c.$. The dots with error bars are data and the lines show the fit to the data. The solid lines (blue) describe the total fits, the dashed lines (red) describe the signal shapes and the green areas describe the background shapes.

has $\sim 9\%$ events in common with the single-tag analysis, so the two analyses are almost statistically independent and can be combined into a weighted average. The combined pole mass and width are $(3882.2 \pm 1.1 \pm 1.5)$ MeV/ c^2 and $(26.5 \pm 1.7 \pm 2.1)$ MeV, respectively. The combined production rate $\sigma(e^+e^- \rightarrow \pi^\mp Z_c(3900)^\pm) \times \mathcal{B}(Z_c(3900)^\pm \rightarrow (D\bar{D}^*)^\pm)$ is $(104.4 \pm 4.8 \pm 8.4)$ pb at $\sqrt{s}=4.26$ GeV.

In an analysis of $e^+e^- \rightarrow \pi^0(D\bar{D}^*)^0$, the $Z_c(3900)^0 \rightarrow (D\bar{D}^*)^0$ is also observed³¹ and agree with the expectation from isospin symmetry.

3.1.3. The quantum numbers

In both the single-tag and double-tag analyses of $Z_c(3900) \rightarrow D\bar{D}^* + c.c.$,^{29,30} by checking the angular distribution of the π accompanying the $Z_c(3900)$, BESIII finds that the spin-parity $J^P = 1^+$ of the $Z_c(3900)$ is favored over $J^P = 0^-$ and 1^- ($J^P = 0^+$ is not allowed due to spin-parity conservation in $Z_c(3900) \rightarrow \pi J/\psi$), but $J > 1$ cannot be ruled out by simply checking one angular distribution.

BESIII determines the spin-parity of the $Z_c(3900)$ based on a PWA of $e^+e^- \rightarrow \pi^+\pi^- J/\psi$ events at $\sqrt{s} = 4.23$ and 4.26 GeV.³² Following the event selection reported in Ref. 11, the numbers of selected candidate events are 4154 at $\sqrt{s} =$

4.23 GeV and 2447 at $\sqrt{s} = 4.26$ GeV, with 365 and 272 background events, respectively, estimated by using the J/ψ mass sidebands.

Amplitudes of the PWA are constructed with the helicity-covariant method.³³ The process $e^+e^- \rightarrow \pi^+\pi^-J/\psi$ is assumed to proceed via the $Z_c(3900)$ resonance, *i.e.*, $e^+e^- \rightarrow \pi^\pm Z_c(3900)^\mp$, $Z_c(3900)^\mp \rightarrow \pi^\mp J/\psi$, and via the non- $Z_c(3900)$ decay $e^+e^- \rightarrow RJ/\psi$, $R \rightarrow \pi^+\pi^-$, with $R = \sigma, f_0(980), f_2(1270)$, and $f_0(1370)$. In the fit, the $Z_c(3900)$ line shape is described with a Flatté-like formula taking into account the fact that the $Z_c(3900)^\pm$ decays are dominated by the final states $(D\bar{D}^*)^\pm$ ^{29,30} and $\pi^\pm J/\psi$.¹¹ All processes are added coherently to obtain the total amplitude.

The fit indicates that the spin-parity $J^P = 1^+$ of the $Z_c(3900)$ are favored by more than 7σ over other quantum numbers ($0^-, 1^-, 2^-,$ and 2^+), as can be seen in Fig. 5 for a $Z_c(3900)$ enriched sample ($m_{J/\psi\pi^\pm} \in (3.86, 3.92)$ GeV/ c^2). Figure 6 shows projections of the fit results with $J^P = 1^+$ for the $Z_c(3900)$ state. The pole mass of the $Z_c(3900)$ is measured as $(3881.2 \pm 4.2 \pm 52.7)$ MeV/ c^2 and pole width $(51.8 \pm 4.6 \pm 36.0)$ MeV. The Born cross sections for $e^+e^- \rightarrow \pi^+Z_c(3900)^- + c.c. \rightarrow \pi^+\pi^-J/\psi$ are measured to be $(21.8 \pm 1.0 \pm 4.4)$ pb at $\sqrt{s} = 4.23$ GeV and $(11.0 \pm 1.2 \pm 5.4)$ pb at $\sqrt{s} = 4.26$ GeV.

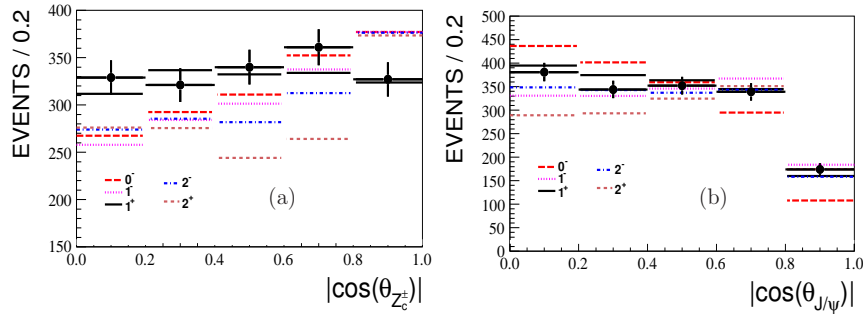


Fig. 5. Polar angle distribution of $Z_c(3900)^\pm$ in $e^+e^- \rightarrow \pi^+Z_c(3900)^- + c.c.$ (a), and helicity angle distribution of J/ψ in the $Z_c(3900)^\pm \rightarrow \pi^\pm J/\psi$ (b). The dots with error bars are the $Z_c(3900)$ enriched sample, and compared with the fits with different J^P hypotheses.

3.1.4. Evidence for $Z_c(3900) \rightarrow \rho\eta_c$

BESIII searches for $e^+e^- \rightarrow \pi^+\pi^-\pi^0\eta_c$ and intermediate states decay into $\rho\eta_c$ with data collected at 4.23, 4.26, and 4.36 GeV.³⁴ In this analysis, η_c is reconstructed with 9 hadronic final states: $p\bar{p}$, $2(K^+K^-)$, $K^+K^-\pi^+\pi^-$, $K^+K^-\pi^0$, $p\bar{p}\pi^0$, $K_S^0K^\pm\pi^\mp$, $\pi^+\pi^-\eta$, $K^+K^-\eta$, and $\pi^+\pi^-\pi^0\pi^0$.

Clear signal of $e^+e^- \rightarrow \pi^+\pi^-\pi^0\eta_c$ is observed at $\sqrt{s} = 4.23$ GeV. The $Z_c(3900/4020)^\pm \rightarrow \rho^\pm\eta_c$ signals are examined after requiring that the invariant mass of the η_c candidate is within the η_c signal region and the invariant mass of

12 Chang-Zheng Yuan

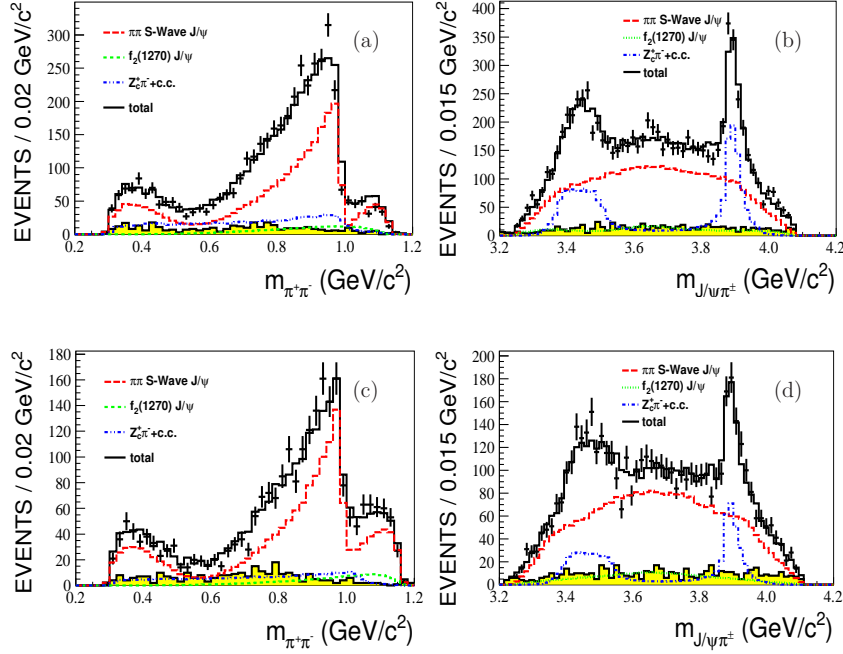


Fig. 6. Projections to $m_{\pi^+\pi^-}$ (a, c) and $m_{J/\psi\pi^\pm}$ (b, d) of the fit results with $J^P = 1^+$ for the $Z_c(3900)$, at $\sqrt{s} = 4.23$ GeV (a, b) and 4.26 GeV (c, d). The points with error bars are data, and the black histograms are the total fit results. The shaded histograms denote backgrounds. Plots (b) and (d) are filled with two entries ($m_{J/\psi\pi^+}$ and $m_{J/\psi\pi^-}$) per event.

$\pi^\pm\pi^0$ is within the ρ^\pm signal region. The recoil mass of the remaining π^\mp (equivalent to the invariant mass of $\rho^\pm\eta_c$) is shown in Fig. 7 for the data at $\sqrt{s} = 4.23$ GeV, the $Z_c(3900)^\pm$ signal is found while there is no significant $Z_c(4020)^\pm$ signal. The $\rho^\pm\eta_c$ invariant mass distribution is fitted with the contributions from $Z_c(3900)$ and $Z_c(4020)$ together with a smooth background. 240 ± 56 $Z_c(3900)^\pm$ events is observed with a statistical significance of 4.3σ (3.9σ including the systematical uncertainty). The $Z_c(3900)$ signals at other c.m. energies and the $Z_c(4020)$ signals at all the c.m. energies are not statistically significant.

The cross section is measured as $\sigma(e^+e^- \rightarrow \pi^\mp Z_c(3900)^\pm \rightarrow \pi^\mp \rho^\pm \eta_c) = (47 \pm 11 \pm 11)$ pb at $\sqrt{s} = 4.23$ GeV. This result is equal within errors to the cross section of $e^+e^- \rightarrow \pi^+\pi^-\pi^0\eta_c$, which is $(46 \pm 12 \pm 10)$ pb. This indicates that the $e^+e^- \rightarrow \pi^+\pi^-\pi^0\eta_c$ process is saturated by the $e^+e^- \rightarrow \pi^\mp Z_c(3900)^\pm \rightarrow \pi^\mp \rho^\pm \eta_c$. No signal is observed at $\sqrt{s} = 4.26$ and 4.36 GeV and the upper limits of the production cross sections at the 90% confidence level (C.L.) are determined.

Using the results from Ref. 32, the ratio of the branching fractions of different $Z_c(3900)^\pm$ decays is calculated as $R_{Z_c(3900)} = \frac{B(Z_c(3900) \rightarrow \rho\eta_c)}{B(Z_c(3900) \rightarrow \pi J/\psi)} = 2.1 \pm 0.8$ at $\sqrt{s} = 4.23$ GeV and less than 6.4 at $\sqrt{s} = 4.26$ GeV at the 90% C.L. The theoretical

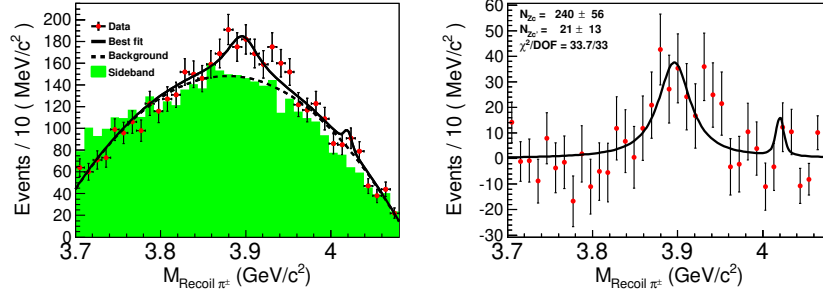


Fig. 7. The π^\pm recoil mass distribution in $e^+e^- \rightarrow \pi^\pm \rho^\mp \eta_c$ at $\sqrt{s} = 4.23$ GeV and the fit with $Z_c(3900)/4020^\pm$ signals (left panel); and the same plot with background subtracted (right panel). Dots with error bars are data, shaded histogram is from η_c sidebands, normalized to the number of backgrounds from the fit, the solid lines are total fit and the dotted line is background.

predictions for this ratio varies depending on model assumptions and ranges from a few per cent to a few hundreds.^{35–40}

3.1.5. Hint for $Z_c(3900) \rightarrow \pi h_c$

BESIII measured cross sections of $e^+e^- \rightarrow \pi^+\pi^-h_c$ at c.m. energies of 3.90–4.42 GeV with $h_c \rightarrow \gamma\eta_c$ and η_c decays into 16 hadronic final states.²¹ Intermediate states were studied by examining the Dalitz plot of the selected $\pi^+\pi^-h_c$ candidate events. While a new resonance $Z_c(4020)$ (see Sec. 3.2.1) is observed, there is only a faint signal at around 3.9 GeV/ c^2 (inset of Fig. 8 (left)), which could be $Z_c(3900)$.

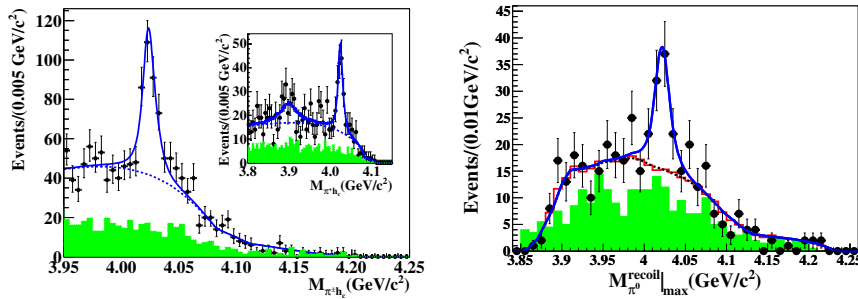


Fig. 8. Sum of the simultaneous fits to the $M(\pi^\pm h_c)$ (left panel) and $M(\pi^0 h_c)$ (right panel) distributions from $e^+e^- \rightarrow \pi^+\pi^-h_c$ and $\pi^0\pi^0h_c$, respectively, at 4.23, 4.26, and 4.36 GeV in the BESIII data; the inset in the left panel shows the sum of the simultaneous fit to the $M(\pi^\pm h_c)$ distributions at 4.23 and 4.26 GeV with $Z_c(3900)$ and $Z_c(4020)$. Dots with error bars are data; shaded histograms are normalized sideband background; the solid curves show the total fit, and the dotted curves the backgrounds from the fit.

An unbinned maximum likelihood fit was applied to the $M(\pi^\pm h_c)$ distribution assuming there are both $Z_c(4020)$ and $Z_c(3900)$ contributions with the mass

and width of the latter fixed to the BESIII measurements.¹¹ The fit results in a statistical significance of 2.1σ (see the inset of Fig. 8 (left)) for the $Z_c(3900)$. At the 90% C.L., the upper limits on the production cross sections are set to $\sigma(e^+e^- \rightarrow \pi^\pm Z_c(3900)^\mp \rightarrow \pi^+\pi^-h_c) < 13$ pb at 4.23 GeV and < 11 pb at 4.26 GeV. These are lower than those of $Z_c(3900) \rightarrow \pi^\pm J/\psi$.³²

3.1.6. Summary on the $Z_c(3900)$

From the above studies, we conclude that the $Z_c(3900)$ is an isovector state with positive G -parity and spin-parity $J^P = 1^+$. It decays into $\pi J/\psi$ and $D\bar{D}^*$, and it may also decay into $\rho\eta_c$ and πh_c final states. The neutral $Z_c(3900)$ has a negative C -parity.

Although the mass and width are reported in many measurements, in most of the cases the interference between the $Z_c(3900)$ and other amplitudes is not considered properly. The most reliable measurement is from the PWA of the $e^+e^- \rightarrow \pi^+\pi^-J/\psi$ mode,³² with the pole mass of $(3881.2 \pm 4.2 \pm 52.7)$ MeV/ c^2 and pole width of $(51.8 \pm 4.6 \pm 36.0)$ MeV. The errors are still large, dominated by the uncertainties in the parametrization of the $\pi^+\pi^-$ S-wave amplitudes. The assumption that $Z_c(3900)$ decays dominantly into $\pi J/\psi$ and $D\bar{D}^*$ in PWA may also introduce bias, as the $\rho\eta_c$ mode has been observed with a larger decay rate than $\pi J/\psi$, and there could be other decay modes such as πh_c , $\pi\psi(2S)$ and so on.

The reported production cross section for $e^+e^- \rightarrow \pi^+Z_c(3900)^- + c.c.$ suffers from the same problems mentioned in the $Z_c(3900)$ mass and width determination. The only reliable measurement is the product cross section of $e^+e^- \rightarrow \pi^+Z_c(3900)^- + c.c. \rightarrow \pi^+\pi^-J/\psi$ determined from PWA which is $(21.8 \pm 1.0 \pm 4.4)$ pb at $\sqrt{s} = 4.23$ GeV and $(11.0 \pm 1.2 \pm 5.4)$ pb at $\sqrt{s} = 4.26$ GeV.³² It seems that the $Z_c(3900)$ is produced at 4.23 GeV twice as much as that at 4.26 GeV. It would be very important to measure the $Z_c(3900)$ production cross sections at other c.m. energies, to check if the line shape of $e^+e^- \rightarrow \pi Z_c(3900)$ is the same as that of $e^+e^- \rightarrow \pi^+\pi^-J/\psi$. This will be an important piece of information in understanding the nature of the $Z_c(3900)$ and the production mechanism.

Although BESIII also searched for the $Z_c(3900)$ decays into isospin violating mode $\eta J/\psi$ ⁴¹ and light hadron final state $\omega\pi$,⁴² it is not surprising that the decays are not observed and the upper limits of the decay rates are one order of magnitude or even smaller than $Z_c(3900) \rightarrow \pi J/\psi$, as expected naively.

3.2. The $Z_c(4020)$

3.2.1. Observation of the $Z_c(4020)$

As has been mentioned in Sec. 3.1.5, BESIII measures cross sections of $e^+e^- \rightarrow \pi^+\pi^-h_c$ at c.m. energies of 3.90–4.42 GeV.²¹ Intermediate states are studied by

examining the Dalitz plot of the selected $\pi^+\pi^-h_c$ candidate events. The h_c signal is selected using $3.518 < M_{\gamma\eta_c} < 3.538$ GeV/ c^2 , and $\pi^+\pi^-h_c$ samples of 859 events at 4.23 GeV, 586 events at 4.26 GeV, and 469 events at 4.36 GeV are obtained with purities of about $\sim 65\%$. Although there are no clear structures in the $\pi^+\pi^-$ system, there is distinct evidence for an exotic charmonium-like structure in the $\pi^\pm h_c$ system, as clearly shown in the Dalitz plot (Fig. 9). Figure 8 (left) shows the projection of the $M(\pi^\pm h_c)$ (two entries per event) distribution for the signal events, as well as the background events estimated from normalized h_c mass sidebands. There is a significant peak at around 4.02 GeV/ c^2 ($Z_c(4020)$), and there are also some events at around 3.9 GeV/ c^2 which could be $Z_c(3900)$. The individual datasets at $\sqrt{s} = 4.23, 4.26,$ and 4.36 GeV show similar structures.

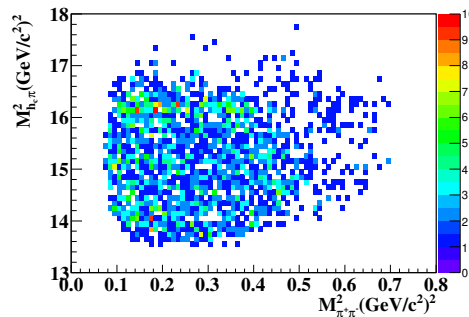


Fig. 9. Dalitz plot ($M^2_{\pi^+h_c}$ vs. $M^2_{\pi^+\pi^-}$) for selected $e^+e^- \rightarrow \pi^+\pi^-h_c$ events, summed over all energy points.

An unbinned maximum likelihood fit is applied to the $M(\pi^\pm h_c)$ distribution summed over the 16 η_c decay modes. The data at 4.23, 4.26, and 4.36 GeV are fitted simultaneously to the same signal function with common mass and width. Figure 8 (left) shows the fitted results. The mass and width of $Z_c(4020)$ are measured to be $(4022.9 \pm 0.8 \pm 2.7)$ MeV/ c^2 and $(7.9 \pm 2.7 \pm 2.6)$ MeV, respectively. The statistical significance of the $Z_c(4020)$ signal is found to be greater than 8.9σ .

The numbers of $Z_c(4020)$ events are determined to be 114 ± 25 , 72 ± 17 , and 67 ± 15 at 4.23, 4.26, and 4.36 GeV, respectively. The cross sections are calculated to be $\sigma(e^+e^- \rightarrow \pi^\pm Z_c(4020)^\mp \rightarrow \pi^+\pi^-h_c) = (8.7 \pm 1.9 \pm 2.8 \pm 1.4)$ pb at 4.23 GeV, $(7.4 \pm 1.7 \pm 2.1 \pm 1.2)$ pb at 4.26 GeV, and $(10.3 \pm 2.3 \pm 3.1 \pm 1.6)$ pb at 4.36 GeV, where the first errors are statistical, the second ones systematic, and the third ones from the uncertainty in $\mathcal{B}(h_c \rightarrow \gamma\eta_c)$.¹

BESIII also observes $e^+e^- \rightarrow \pi^0\pi^0h_c$ at $\sqrt{s} = 4.23, 4.26,$ and 4.36 GeV for the first time.⁴³ The measured Born cross sections are about half of those for $e^+e^- \rightarrow \pi^+\pi^-h_c$, which agree with expectations based on isospin symmetry within systematic uncertainties. $Z_c(4020)^0$, the neutral isospin partner of the $Z_c(4020)^\pm$

is observed in $\pi^0 h_c$ invariant mass distribution (Fig. 8 (right)). This observation indicates that there are no anomalously large isospin violations in $\pi^+ \pi^- h_c$ and $\pi Z_c(4020)$ systems, and $Z_c(4020)$ is an isovector state.

3.2.2. Observation of $Z_c(4020) \rightarrow D^* \bar{D}^*$

The $Z_c(4020)$ is very close to and is above the $D^* \bar{D}^*$ threshold of $4.02 \text{ GeV}/c^2$, so it may couple to $D^* \bar{D}^*$ final state. The BESIII experiment studies the $e^+ e^- \rightarrow (D^* \bar{D}^*)^\pm \pi^\mp$ process using data at $\sqrt{s} = 4.26 \text{ GeV}$.⁴⁴ Based on a partial reconstruction technique (only the bachelor π^\mp , one charged D , and one π^0 from D^* decays are reconstructed), the Born cross section is measured to be $(137 \pm 9 \pm 15) \text{ pb}$. A structure near the $(D^* \bar{D}^*)^\pm$ threshold in the π^\mp recoil mass spectrum is observed (see Fig. 10 (left)). The measured mass and width of the structure are $(4026.3 \pm 2.6 \pm 3.7) \text{ MeV}/c^2$ and $(24.8 \pm 5.6 \pm 7.7) \text{ MeV}$, respectively, from the fit with a constant-width BW function for the signal, and the statistical significance is 13σ . From the fit results, 401 ± 47 $Z_c(4020)$ signal events are obtained, and the associated ratio of the production rates $\frac{\sigma(e^+ e^- \rightarrow Z_c(4020)^\pm \pi^\mp \rightarrow (D^* \bar{D}^*)^\pm \pi^\mp)}{\sigma(e^+ e^- \rightarrow (D^* \bar{D}^*)^\pm \pi^\mp)}$ is determined to be $0.65 \pm 0.09 \pm 0.06$.

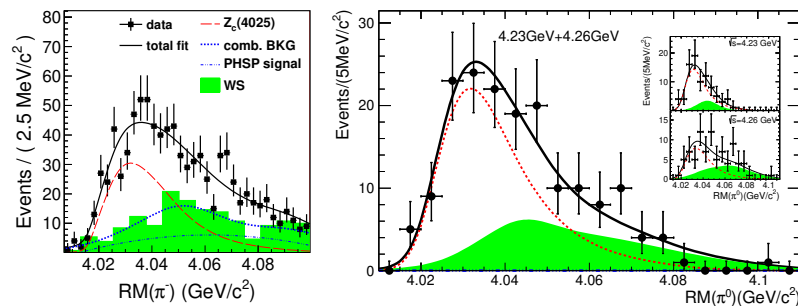


Fig. 10. Unbinned maximum likelihood fit to the π^\mp recoil mass spectrum (left) in $e^+ e^- \rightarrow (D^* \bar{D}^*)^\pm \pi^\mp$ at $\sqrt{s} = 4.26 \text{ GeV}$, and to the π^0 recoil mass spectrum (right) in $e^+ e^- \rightarrow (D^* \bar{D}^*)^0 \pi^0$ at $\sqrt{s} = 4.23$ and 4.26 GeV at BESIII.

The processes $e^+ e^- \rightarrow (D^{*0} \bar{D}^{*0}) \pi^0$ and $(D^{*+} D^{*-}) \pi^0$ are also studied at BESIII to search for the neutral partner of the $Z_c(4020)$ state.⁴⁵ In this analysis, two D mesons are reconstructed together with the bachelor π^0 with data at $\sqrt{s} = 4.23$ and 4.26 GeV . The $Z_c(4020)^0$ is observed in the π^0 recoil mass spectrum (see Fig. 10 (right)). The mass spectrum is fitted with the incoherent sum of a BW function with a mass-dependent width and MC simulated background shape. The mass and width of its pole position are determined to be $(4025.5^{+2.0}_{-4.7} \pm 3.1) \text{ MeV}/c^2$ and $(23.0 \pm 6.0 \pm 1.0) \text{ MeV}$, respectively.

From the simultaneous fit, 69.5 ± 9.2 and 46.1 ± 8.5 $Z_c(4020)^0$ signal events are obtained at 4.23 and 4.26 GeV , respectively, with a statistical significance of

5.9 σ . The Born cross section $\sigma(e^+e^- \rightarrow Z_c(4020)^0\pi^0 \rightarrow (D^{*0}\bar{D}^{*0} + D^{*+}D^{*-})\pi^0)$ is measured to be $(61.6 \pm 8.2 \pm 9.0)$ pb at 4.23 GeV and $(43.4 \pm 8.0 \pm 5.4)$ pb at 4.26 GeV. The ratio $\frac{\sigma(e^+e^- \rightarrow Z_c(4020)^0\pi^0 \rightarrow (D^*\bar{D}^*)^0\pi^0)}{\sigma(e^+e^- \rightarrow Z_c(4020)^+\pi^- \rightarrow (D^*\bar{D}^*)^+\pi^-)}$ is compatible with unity at $\sqrt{s} = 4.26$ GeV, which is expected from isospin symmetry. This also confirms the isospin of the $Z_c(4020)$ is one.

3.2.3. Search for $Z_c(4020) \rightarrow \pi J/\psi$

As has been described in Sec. 3.1.3, using the two data sets at $\sqrt{s} = 4.23$ and 4.26 GeV, BESIII also searches for the process $e^+e^- \rightarrow Z_c(4020)^+\pi^- + c.c. \rightarrow \pi^+\pi^- J/\psi$ in the PWA, with the $Z_c(4020)^\pm$ assumed to be a 1^+ state added in the global fit. In the PWA, its mass is taken from Ref. 21, and its width is taken as the observed value, which includes the detector resolution. The statistical significance for $Z_c(4020)^\pm \rightarrow J/\psi\pi^\pm$ is found to be 3σ in the combined data. The Born cross sections are measured to be (0.2 ± 0.1) pb at $\sqrt{s} = 4.23$ GeV and (0.8 ± 0.4) pb at $\sqrt{s} = 4.26$ GeV, and the corresponding upper limits at the 90% C.L. are estimated to be 0.9 and 1.4 pb, respectively.

3.2.4. Search for $Z_c(4020) \rightarrow \rho\eta_c$

As has been shown in Fig. 7, no statistically significant $Z_c(4020)^\pm$ signal is observed in the $\rho\eta_c$ decay mode at $\sqrt{s} = 4.23$ GeV.³⁴ The fit to the invariant mass distribution yields 21 ± 13 signal $Z_c(4020)^\pm$ events with a statistical significance of only 1.0σ . The upper limit of the production cross section at the 90% C.L. is determined to be 16 pb. The $Z_c(4020)^\pm$ signal at $\sqrt{s} = 4.26$ and 4.36 GeV are not statistically significant either, and the upper limits of the production cross section are determined to be 9 and 11 pb, respectively, at the 90% C.L.

By comparing with the cross sections of $e^+e^- \rightarrow \pi^\mp Z_c(4020)^\pm \rightarrow \pi^+\pi^- h_c$, one measures the upper limit on the ratio of the $Z_c(4020)$ decay branching fractions, $R_{Z_c(4020)} = \mathcal{B}(Z_c(4020)^\pm \rightarrow \rho^\pm\eta_c)/\mathcal{B}(Z_c(4020)^\pm \rightarrow \pi^\pm h_c) < 1.9, 1.2,$ and 1.0 at c.m. energies of 4.23, 4.26, and 4.36 GeV, respectively, at the 90% C.L. The ratio is smaller than the calculations based on tetraquark model while not in contradiction with the molecule model calculation which is about two orders of magnitude smaller than the current upper limit.³⁵

3.2.5. Summary on the $Z_c(4020)$

From the above studies, we conclude that the $Z_c(4020)$ is an isovector state with positive G -parity, similar to the $Z_c(3900)$ state. The spin-parity quantum numbers of the $Z_c(4020)$ are not measured, but $J^P = 1^+$ are assumed in all the analyses. $Z_c(4020)$ decays into πh_c and $D^*\bar{D}^*$. It may also decay into $\pi J/\psi$ final state but the decay into $\rho\eta_c$ is not observed. The neutral $Z_c(4020)$ has a negative C -parity.

Although the mass and width are reported in both $\pi^+\pi^-h_c$ and $D^*\bar{D}^*$ final states, the comparison of the numbers is not straightforward. The reported values depend on different assumptions on the signal shape in different analysis and the interference between $Z_c(4020)$ and other amplitudes is neglected. In the $\pi D^*\bar{D}^*$ analyses,^{44,45} the $Z_c(4020)^\pm$ and $Z_c(4020)^0$ are parametrized with different line shapes and the pole mass and width are reported in the latter case. In addition, the fractions of non- $Z_c(4020)$ events in $e^+e^- \rightarrow \pi D^*\bar{D}^*$ are quite different in charged and neutral modes. All these suggest that improved measurements of $e^+e^- \rightarrow \pi D^*\bar{D}^*$, both charged and neutral modes, using more D -tag modes and data at other c.m. energies are necessary.

The most reliable measurement is probably from $e^+e^- \rightarrow \pi^+\pi^-h_c$ mode.²¹ Although the resonance is parametrized with a constant-width BW function and the interference with non- $Z_c(4020)$ amplitudes is also neglected, the fact that the width is very narrow makes the line shape distortion due to these above effects not very significant. The mass and width are measured to be $(4022.9 \pm 0.8 \pm 2.7)$ MeV/ c^2 and $(7.9 \pm 2.7 \pm 2.6)$ MeV, respectively, in this mode. Of course, a coupled channel analysis of $\pi^+\pi^-h_c$ and $\pi D^*\bar{D}^*$ modes will give more reliable measurements of the resonant parameters.

The production cross section for $e^+e^- \rightarrow \pi Z_c(4020)$ suffers from the same problems mentioned in the $Z_c(4020)$ mass and width determination. It would be very important to measure the $Z_c(4020)$ production cross sections as a function of the c.m. energy with PWA, to check if $e^+e^- \rightarrow \pi Z_c(4020)$ is from continuum production or from decays of some resonant structures, such as the $Y(4220)$ and $Y(4390)$ observed in $e^+e^- \rightarrow \pi^+\pi^-h_c$,⁴⁶ this will be an important piece of information in understanding the nature of the $Z_c(4020)$ and the production mechanism.

3.3. The Z_c structures in $\pi\psi(2S)$ system

3.3.1. The $Z_c(4430)$

The Belle collaboration first reported evidence for a narrow $Z_c(4430)^-$ peak, with mass $M = (4433 \pm 4 \pm 2)$ MeV/ c^2 and width $\Gamma = (45_{-13}^{+18+30})$ MeV, in the $\pi^-\psi(2S)$ invariant mass distribution in $B \rightarrow K\pi^-\psi(2S)$ decays.¹⁷ The BaBar collaboration did the same analyses,⁴⁷ but did not confirm its existence. On the other hand, the BaBar's results did not contradict the Belle observation due to low statistics. This has been an open question for a very long time since there were no new data available until recently.

To take into account the interference effect between the $Z_c(4430)^-$ and the K^* intermediate states in $B \rightarrow K\pi^-\psi(2S)$ decays, the Belle collaboration updated their $Z_c(4430)^-$ results with a four-dimensional (4D) amplitude analysis.¹⁸ The $Z_c(4430)^-$ is observed with a significance of 5.2σ , a much larger mass of $(4485 \pm 22_{-11}^{+28})$ MeV/ c^2 , and a large width of (200_{-46-35}^{+41+26}) MeV. The product branching

fractions are measured to be $\mathcal{B}(B^0 \rightarrow Z_c(4430)^- K^+) \times \mathcal{B}(Z_c(4430)^- \rightarrow \pi^- \psi(2S)) = (6.0_{-2.0}^{+1.7+2.5}) \times 10^{-5}$, and spin-parity $J^P = 1^+$ is favored over the other assignments by more than 3.4σ . This was confirmed recently by the LHCb experiment.¹⁹

LHCb reported a 4D model-dependent amplitude fit to a sample of $25,176 \pm 174$ $B^0 \rightarrow K^+ \pi^- \psi(2S)$, $\psi(2S) \rightarrow \mu^+ \mu^-$ events reconstructed in a 3 fb^{-1} data sample collected at $\sqrt{s} = 7$ and 8 TeV. The order-of-magnitude increase in signal yield over the Belle measurement¹⁸ improves sensitivity to the quantum numbers of the $Z_c(4430)^-$ and allows a measurement of the Argand plot.

In the amplitude fit, the Z_c^- amplitude is represented by a BW function, the measured mass of $(4475 \pm 7_{-25}^{+15}) \text{ MeV}/c^2$ and width of $(172 \pm 13_{-34}^{+37}) \text{ MeV}$ are consistent with, but more precise than, the Belle results.¹⁸ Relative to $J^P = 1^+$, LHCb data rule out the 0^- , 1^- , 2^+ and 2^- hypotheses by at least 9σ , and establishes the spin-parity of the $Z_c(4430)$ to be 1^+ .

In addition, LHCb measures Argand plot of the Z_c^- amplitude as a function of $M_{\pi\psi(2S)}$ (shown in Fig. 11), which is consistent with a rapid change of the $Z_c(4430)^-$ phase when its magnitude reaches the maximum, an expected behavior of a resonance. This is the first time an Argand plot is measured for an exotic charmonium-like state.

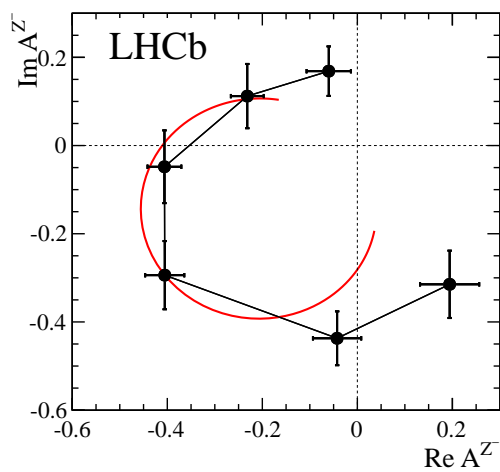


Fig. 11. The Argand plot of the $Z_c(4430)$ amplitudes (points with error bars, $M_{\pi\psi(2S)}^2$ increases counterclockwise). The curve is the prediction from a BW function with mass and width of $4475 \text{ MeV}/c^2$ and 172 MeV , respectively.

3.3.2. The Z_c structure in $e^+e^- \rightarrow \pi^+\pi^-\psi(2S)$

In a study of $e^+e^- \rightarrow \pi^+\pi^-\psi(2S)$, charged structure at $4.03 \text{ GeV}/c^2$ is observed at Belle and BESIII experiments.

Using the 980 fb^{-1} full data sample, Belle updated the measurement of $e^+e^- \rightarrow \pi^+\pi^-\psi(2S)$ using ISR technique with two $\psi(2S)$ decay modes,²² namely, $\pi^+\pi^-J/\psi$ and $\mu^+\mu^-$. Possible charged charmonium-like structures in $\pi^\pm\psi(2S)$ final states from the $Y(4360)$ or $Y(4660)$ decays are searched for with the selected candidate events. Figure 12 shows the sum of $M_{\pi^-\psi(2S)}$ and $M_{\pi^+\psi(2S)}$ distributions in $Y(4360)$ decays ($4.0 < M_{\pi^+\pi^-\psi(2S)} < 4.5 \text{ GeV}/c^2$) from both the $\pi^+\pi^-J/\psi$ and the $\mu^+\mu^-$ modes. An unbinned maximum-likelihood fit is performed on the distribution of $M_{\text{max}}(\pi^\pm\psi(2S))$, the maximum of $M(\pi^+\psi(2S))$ and $M(\pi^-\psi(2S))$, simultaneously with both modes. The excess is parameterized with a BW function and the non-resonant non-interfering background with a second-order polynomial function. The fit yields a mass of $(4054 \pm 3 \pm 1) \text{ MeV}/c^2$ and a width of $(45 \pm 11 \pm 6) \text{ MeV}$. The statistical significance of the signal is 3.5σ .

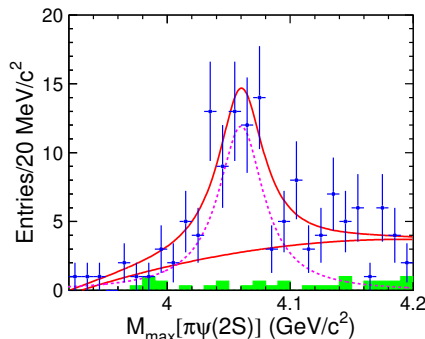


Fig. 12. The distribution of $M_{\text{max}}(\pi^\pm\psi(2S))$ from $Y(4360)$ decays in $e^+e^- \rightarrow \pi^+\pi^-\psi(2S)$ at Belle. The points with error bars represent the data; the histogram is from the sidebands and normalized to the signal region; the solid curve is the best fit and the dashed curve is the signal parametrized with a BW function.

BESIII studies the process $e^+e^- \rightarrow \pi^+\pi^-\psi(2S)$ using 5.1 fb^{-1} of data at c.m. energies from 4.0 to 4.6 GeV.²³ Intermediate states are investigated in the data samples that have large integrated luminosity. The Dalitz plot and the corresponding one-dimensional projections are shown in Fig. 13 for data at $\sqrt{s} = 4.416 \text{ GeV}$, a prominent narrow structure is observed around $4.03 \text{ GeV}/c^2$ in the $M(\pi^\pm\psi(2S))$ spectrum.

An unbinned maximum likelihood fit to the Dalitz plot is applied at BESIII. Assuming an intermediate Z_c state in $\pi\psi(2S)$ system with spin-parity $J^P = 1^+$, the Dalitz plot is parameterized by the incoherent sum of the process $\pi Z_c \rightarrow \pi^+\pi^-\psi(2S)$ and the direct process $e^+e^- \rightarrow \pi^+\pi^-\psi(2S)$. The fit yields a mass of $M = (4032.1 \pm 2.4) \text{ MeV}/c^2$ and a width of $\Gamma = (26.1 \pm 5.3) \text{ MeV}$ for the inter-

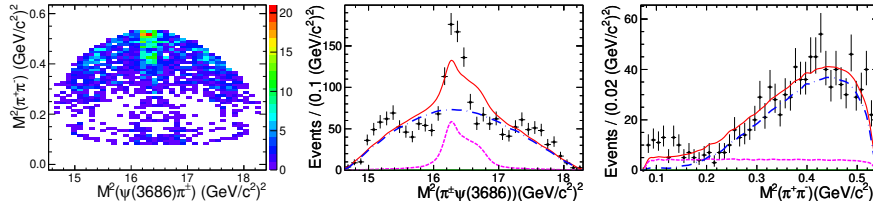


Fig. 13. Dalitz plot of $e^+e^- \rightarrow \pi^+\pi^-\psi(2S)$ at $\sqrt{s} = 4.416$ GeV (two entries per event) from BESIII. Dots with errors are data. The solid curves (red) are projections from the fit; the dashed curves (pink) show the shape of the intermediate state; the dash-dotted curves (blue) show the shape from the direct process $e^+e^- \rightarrow \pi^+\pi^-\psi(2S)$ obtained from MC model.

mediate state with a significance of 9.2σ . The fit projections on $M^2(\pi^\pm\psi(2S))$ and $M^2(\pi^+\pi^-)$ are shown in Fig. 13. It is observed that the fit curve does not match data well, thus BESIII reported statistical errors only for the parameters of the Z_c structure.

The BESIII data are refitted with a similar model as is used in the description of the Z_b states in $\Upsilon(5S)$ decays.⁴⁸ This fit considers the interference effect between the $\pi^+\pi^-$ amplitude and the Z_c amplitude properly. It is found that the structure can be described well with a charged state with a mass of (4019.0 ± 1.9) MeV/ c^2 and width of (29 ± 4) MeV, or the same state observed in $\pi^+\pi^-h_c$ final state, $Z_c(4020)$,²¹ and the fit quality is much improved. The fraction of $\pi Z_c(4020) \rightarrow \pi^+\pi^-\psi(2S)$ is $(12.0 \pm 3.7)\%$ of the total $e^+e^- \rightarrow \pi^+\pi^-\psi(2S)$ cross section, that is, $\sigma(e^+e^- \rightarrow \pi^+Z_c(4020)^- + c.c. \rightarrow \pi^+\pi^-\psi(2S)) = (5.1 \pm 1.6)$ pb. Unfortunately there is no corresponding cross section of $e^+e^- \rightarrow \pi^+Z_c(4020)^- + c.c. \rightarrow \pi^+\pi^-h_c$ at the same energy to compare with. If we take the cross section of $e^+e^- \rightarrow \pi^+Z_c(4020)^- + c.c. \rightarrow \pi^+\pi^-h_c$ at 4.36 GeV for comparison, we obtain $\frac{\mathcal{B}(Z_c(4020) \rightarrow \pi\psi(2S))}{\mathcal{B}(Z_c(4020) \rightarrow \pi h_c)} \sim 0.5 \pm 0.3$. It is obvious both $\pi^+\pi^-\psi(2S)$ and $\pi^+\pi^-h_c$ final states need to be further investigated to understand the intermediate structures.

3.4. Summary on the Z_c states

Although many measurements have been performed on the $Z_c(3900)$, $Z_c(4020)$, and $Z_c(4430)$, the experimental information is still not precise enough. From the studies of the $Z_c(4430)$ we know that the resonant parameters may change significantly by doing simple 1D fit to the invariant mass distribution¹⁷ or by doing full amplitude analysis with the interference effects between different amplitudes considered properly.¹⁸ The same thing may happen to the $Z_c(3900)$ and $Z_c(4020)$ cases too. Amplitude analysis of the relevant final states to extract the resonant parameters as well as the couplings to different modes is essential to extract correct information for understanding the nature of these states. In addition, the PWA also allows a measurement of the Argand plot of the Z_c amplitudes, which may be used to discriminate models of the Z_c states.

Comparison of the Z_c with the Z_b states⁴⁹ may help understand these structures too. The decays of $Z_b(10610)$ and $Z_b(10650)$ to $\pi\Upsilon(nS)$ ($n = 1, 2, 3$), $\pi h_b(mP)$ ($m = 1, 2$), $B\bar{B}^* + c.c.$, and $B^*\bar{B}^*$ have been measured while only significant $Z_c(3900) \rightarrow \pi J/\psi$, $D\bar{D}^* + c.c.$ and $Z_c(4020) \rightarrow \pi h_c$, $D^*\bar{D}^*$ are observed; on the other hand, evidence for $Z_c(3900) \rightarrow \rho\eta_c$ is observed while no measurement of $Z_b \rightarrow \rho\eta_b$ is reported yet. Many of these final states can be reached at BESIII and Belle II⁵⁰ in the near future. Needless to say, there are other decay modes to search for, such as final state with D-wave quarkonium state like $\pi\psi(1D)$ and $\pi\Upsilon(1D)$.

The production of the Z_c states as a function of c.m. energy should also be measured in a similar way as has been presented for $Z_c(3900)$ and $Z_c(4020)$ at a few c.m. energies, this may reveal whether these states are from resonance decays or continuum production. So far $Z_c(3900)$ and $Z_c(4020)$ are only observed in e^+e^- annihilation⁵¹ while $Z_c(4430)$ only in B decays. Search for these states in different production modes is of great importance.

4. The $X(3872)$

The $X(3872)$ was observed in $B^\pm \rightarrow K^\pm\pi^+\pi^-J/\psi$ decays 15 years ago at the Belle experiment.⁵² It was confirmed subsequently by several other experiments.⁵³⁻⁵⁵ Since its discovery, the $X(3872)$ state has stimulated special interest for its nature. Both BaBar, Belle, and LHCb reported evidence for $X(3872) \rightarrow \gamma J/\psi$ decay, which supports $X(3872)$ being a C -even state.⁵⁶⁻⁵⁸ The CDF and LHCb experiments determine the spin-parity of the $X(3872)$ to be $J^P = 1^+$, and the $\pi^+\pi^-$ system is dominated by a $\rho^0(770)$ resonance in $X(3872) \rightarrow \pi^+\pi^-J/\psi$.⁵⁹⁻⁶²

The $X(3872)$ is only observed in B meson decays and hadron collisions before. Since the quantum numbers of $X(3872)$ are $J^{PC} = 1^{++}$, it can be produced through the radiative transition of excited vector charmonium or charmonium-like states such as the ψ s and the Y s and the evidence for the $Y(4260) \rightarrow \gamma X(3872)$ is reported by the BESIII experiment.⁶³

4.1. The spin-parity of the $X(3872)$

The spin-parity quantum numbers J^P of the $X(3872)$ are restricted to two possibilities, 1^+ or 2^- , by the CDF experiment, via an analysis of the angular correlations in $X(3872) \rightarrow \pi^+\pi^-J/\psi$ and $J/\psi \rightarrow \mu^+\mu^-$.⁵⁹ Using 1.0 fb^{-1} of pp collision data, LHCb rules out $J^P = 2^-$ by analyzing the angular correlations in the same decay chain, with the $X(3872)$ state produced in $B^+ \rightarrow X(3872)K^+$ decays.⁶⁰ However, these above analyses assumed that the lowest orbital angular momentum between the $X(3872)$ decay products dominates the matrix element.

This assumption is removed later by LHCb in a five-dimensional (5D) angular correlation analysis in $B^+ \rightarrow X(3872)K^+$, $X(3872) \rightarrow \rho^0 J/\psi$, $\rho^0 \rightarrow \pi^+\pi^-$, $J/\psi \rightarrow \mu^+\mu^-$ decays with 1011 ± 38 events selected from 3 fb^{-1} data at 7 and 8 TeV.⁶² This

analysis confirms that the spin, parity, and charge-conjugation of the $X(3872)$ state are 1^{++} , the same quantum numbers as one of the P-wave spin-triplet charmonium state $\chi_{c1}(2P)$. The comparison between data and the fit projections for $J^{PC} = 1^{++}$ is shown in Fig. 14 (left), and the comparison between data and expectation from other spin-parity is shown in Fig. 14 (right). We can see that $J^{PC} = 1^{++}$ describe data very well and other J^{PC} have very different angular distributions.

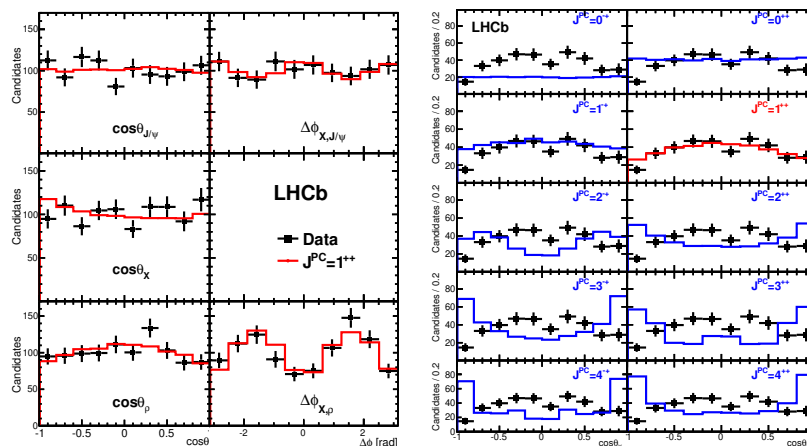


Fig. 14. Background-subtracted distributions of all angles for the data (left panel) and background-subtracted distribution of $\cos\theta_X$ for candidates with $|\cos\theta_\rho| > 0.6$ for the data compared with the expected distributions for various $X(3872)$ J^{PC} assignments (right panel). Points with error bars are LHCb data, and the solid histograms are the fit projections (left panel) and expected distributions (right panel).

4.2. The puzzling radiative transitions $X(3872) \rightarrow \gamma J/\psi$ and $\gamma\psi(2S)$

Radiative decays of the $X(3872)$ to lower mass charmonium states provide crucial information to understand its nature, especially to check if it is a conventional charmonium or an exotic state.

The transition $X(3872) \rightarrow \gamma J/\psi$ was measured by BaBar⁶⁴ (28 ± 7 signal events with a statistical significance of 3.6σ), Belle⁵⁷ (36_{-8}^{+9} signal events with a statistical significance of 5.5σ), and LHCb experiments⁵⁸ (591 ± 48 signal events). So $X(3872) \rightarrow \gamma J/\psi$ is well established.

For $X(3872) \rightarrow \gamma\psi(2S)$, evidence was first reported by BaBar⁶⁴ with 33 ± 8 observed signal events and a statistical significance of 3.5σ . The ratio of the branching fractions is measured to be

$$R = \frac{\mathcal{B}(X(3872) \rightarrow \gamma\psi(2S))}{\mathcal{B}(X(3872) \rightarrow \gamma J/\psi)} = 3.4 \pm 1.4.$$

In a study at the LHCb experiment based on a 3 fb^{-1} data sample at $\sqrt{s} = 7$ and 8 TeV, strong evidence for the decay $X(3872) \rightarrow \gamma\psi(2S)$ was reported together with a measurement of R .⁵⁸ In the data sample, $36.4 \pm 9.0 B^\pm \rightarrow X(3872)K^\pm$, $X(3872) \rightarrow \gamma\psi(2S)$ events are observed with a statistical significance of 4.4σ . LHCb measures

$$R = \frac{\mathcal{B}(X(3872) \rightarrow \gamma\psi(2S))}{\mathcal{B}(X(3872) \rightarrow \gamma J/\psi)} = 2.46 \pm 0.64 \pm 0.29.$$

This result is in good agreement with BaBar's measurement.

In contrast, no significant signal was observed at Belle and an upper limit of $R < 2.1$ was reported at the 90% C.L.⁵⁷ (using the information from Ref. 57, we obtain $R = \frac{\mathcal{B}(X(3872) \rightarrow \gamma\psi(2S))}{\mathcal{B}(X(3872) \rightarrow \gamma J/\psi)} = 0.6 \pm 1.4$ as a good estimation of the central value and uncertainty). Although not in disagreement, BaBar, LHCb, and Belle results do show some tension on the decay rate of $X(3872) \rightarrow \gamma\psi(2S)$.

As the measurements of all the above three experiments agree with each other, we can make a weighted average to give the best estimation of R . Neglecting the small correlated errors in the measurements, we obtain

$$\bar{R} = \frac{\mathcal{B}(X(3872) \rightarrow \gamma\psi(2S))}{\mathcal{B}(X(3872) \rightarrow \gamma J/\psi)} = 2.31 \pm 0.57.$$

This value does not support a pure $\bar{D}^0 D^{*0} + c.c.$ molecule interpretation of the $X(3872)$ state, but agrees with expectations if the $X(3872)$ is a pure charmonium or a mixture of a molecule and a charmonium.^{6,58} Of course many of the calculations have model-dependent parameters, adjustment of the parameters may still reproduce the experimental data.

As there is still no experiment reports $X(3872) \rightarrow \gamma\psi(2S)$ signal with statistical significance larger than 5σ , the existence of this transition still needs further experimental investigation.

4.3. Decay branching fractions of the $X(3872)$

So far, all the $X(3872)$ related measurements are product branching fractions or relative branching ratios since the absolute production rate of the $X(3872)$ is unknown in any of the measurements. The only attempt to measure the production of the $X(3872)$ is via inclusive B decays into an $X(3872)$ and a kaon at BaBar and Belle experiments.

BaBar set an upper limit of the $X(3872)$ production rate in the B -meson decays by measuring the momentum distribution of the inclusive kaon from B -meson decays with $210 \text{ fb}^{-1} \Upsilon(4S)$ data.⁶⁵ $\mathcal{B}(B^- \rightarrow K^- X(3872)) < 3.2 \times 10^{-4}$ at the 90% C.L.

A recent update is from the Belle experiment with the full sample of $772 \times 10^6 B\bar{B}$ pairs ($711 \text{ fb}^{-1} \Upsilon(4S)$ data).⁶⁶ No significant $X(3872)$ signal is observed, and Belle sets a more stringent upper limit

$$\mathcal{B}(B^- \rightarrow K^- X(3872)) < 2.7 \times 10^{-4}$$

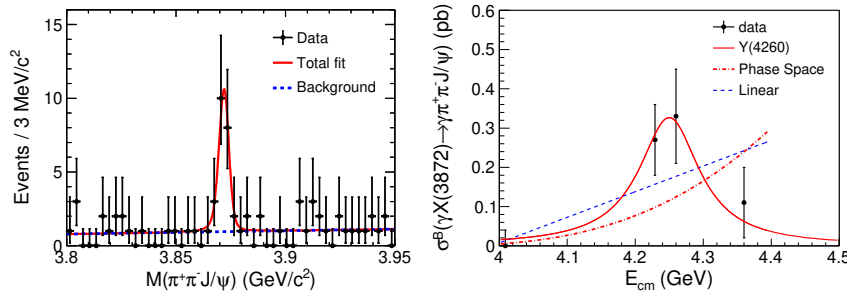


Fig. 15. Left panel: fit the $M(\pi^+\pi^-J/\psi)$ distribution observed at BESIII. Dots with error bars are data, the curves are the best fit. Right panel: fit to $\sigma^B[e^+e^- \rightarrow \gamma X(3872)] \times \mathcal{B}[X(3872) \rightarrow \pi^+\pi^-J/\psi]$ measured by BESIII (dots with error bars) with a $Y(4260)$ resonance (red solid curve), a linear continuum (blue dashed curve), or an $E1$ -transition phase space term (red dotted-dashed curve).

at the 90% C.L., and the central value is $\mathcal{B}(B^- \rightarrow K^- X(3872)) = (1.2 \pm 1.1 \pm 0.1) \times 10^{-4}$.

Together with all the other measurements on the product branching fractions $\mathcal{B}(B^- \rightarrow K^- X(3872)) \cdot \mathcal{B}(X(3872) \rightarrow \text{exclusive})$ (exclusive = $\pi^+\pi^-J/\psi$, $\pi^+\pi^-\pi^0J/\psi$, $\gamma J/\psi$, $\gamma\psi(2S)$, $D^0\bar{D}^{*0} + c.c.$),¹ one obtains

$$2.9\% < \mathcal{B}(X(3872) \rightarrow \pi^+\pi^-J/\psi) < 10\%,$$

$$0.9 \times 10^{-4} < \mathcal{B}(B^- \rightarrow K^- X(3872)) < 2.7 \times 10^{-4},$$

at the 90% C.L.⁶⁷ We find that the decay width of the $X(3872)$ to $\pi^+\pi^-J/\psi$ is larger and the production rate of the $X(3872)$ is smaller than conventional charmonium states such as η_c , $\psi(2S)$, and χ_{c1} .¹ The branching fraction of other $X(3872)$ decay modes can be estimated in a similar way, while it decays dominantly into open charm final state $D^0\bar{D}^{*0} + c.c.$, its decays into each final state with a charmonium is at a few per cent level.

4.4. Observation of $e^+e^- \rightarrow \gamma X(3872)$

BESIII observed $e^+e^- \rightarrow \gamma X(3872) \rightarrow \gamma\pi^+\pi^-J/\psi$, with data collected at 4.23, 4.26, and 4.36 GeV.⁶³

The $M(\pi^+\pi^-J/\psi)$ distribution (summed over all energy points), as shown in Fig. 15 (left), is fitted to extract the mass and signal yield of $X(3872)$ (BESIII experiment is insensitive to the width of the $X(3872)$). The ISR $\psi(2S)$ signal is used to calibrate the absolute mass scale and to extract the resolution difference between data and MC simulation. Figure 15 shows the fitted result: the measured mass of $X(3872)$ is $(3871.9 \pm 0.7 \pm 0.2) \text{ MeV}/c^2$ and the width is found to be less than 2.4 MeV at the 90% C.L. The statistical significance of $X(3872)$ is 6.3σ .

The Born cross section is measured, and the results are listed in Table 2 and plotted in Fig. 15 (right). The energy-dependent cross sections are compared with a $Y(4260)$ resonance (parameters fixed to PDG¹ values), linear continuum, or $E1$ -transition phase space ($\propto E_\gamma^3$) term. The $Y(4260)$ resonance describes the data better than the other two options.

Table 2. The product of the Born cross section $\sigma^B(e^+e^- \rightarrow \gamma X(3872))$ and $\mathcal{B}(X(3872) \rightarrow \pi^+\pi^- J/\psi)$ at different energy points. The upper limits are given at 90% C.L.

\sqrt{s} (GeV)	$\sigma^B[e^+e^- \rightarrow \gamma X(3872)] \cdot \mathcal{B}(X(3872) \rightarrow \pi^+\pi^- J/\psi)$ (pb)
4.009	$0.00 \pm 0.04 \pm 0.01$ or < 0.11
4.229	$0.27 \pm 0.09 \pm 0.02$
4.260	$0.33 \pm 0.12 \pm 0.02$
4.360	$0.11 \pm 0.09 \pm 0.01$ or < 0.36

These observations strongly support the existence of the radiative transition $Y(4260) \rightarrow \gamma X(3872)$. Together with the hadronic transition to the charged charmonium-like state $Z_c(3900)$,^{11,20,27} this suggests that there might be some commonality in the nature of $X(3872)$, $Y(4260)$, and $Z_c(3900)$, and so the model developed to interpret any one of them should also consider the other two.

Combining the measurements at c.m. energies 4.23 and 4.26 GeV with the $e^+e^- \rightarrow \pi^+\pi^- J/\psi$ cross sections at the same energies from BESIII,⁶⁸ we obtain $\sigma^B[e^+e^- \rightarrow \gamma X(3872)] \cdot \mathcal{B}[X(3872) \rightarrow \pi^+\pi^- J/\psi] / \sigma^B(e^+e^- \rightarrow \pi^+\pi^- J/\psi) = (3.7 \pm 0.9) \times 10^{-3}$, under the assumption that $X(3872)$ and $\pi^+\pi^- J/\psi$ are only produced from $Y(4260)$ decays. If we take $\mathcal{B}[X(3872) \rightarrow \pi^+\pi^- J/\psi] = 5\%$ as estimated in previous section, then $\mathcal{R} = \frac{\mathcal{B}[Y(4260) \rightarrow \gamma X(3872)]}{\mathcal{B}(Y(4260) \rightarrow \pi^+\pi^- J/\psi)} \sim 0.1$.

4.5. More studies at BESIII and LHCb?

After 15 years of study, the knowledge on the $X(3872)$ is still very limited, we know it is an isoscalar with $J^{PC} = 1^{++}$, a very precise mass close to the $D^0 \bar{D}^{*0}$ threshold, and a very narrow width. We only have significant observations of its decays into $D^0 \bar{D}^{*0}$, $\pi^+\pi^- J/\psi$, and $\gamma J/\psi$, while the significances of other modes $\pi^+\pi^-\pi^0 J/\psi$ and $\gamma\psi(2S)$ are still less than 5σ .

Since more data have been accumulated at LHCb, some of the measurements can be improved, such as the study of $X(3872) \rightarrow \gamma\psi(2S)$ and possibly search for $X(3872) \rightarrow \pi^+\pi^-\pi^0 J/\psi$ if the π^0 background can be handled properly. The BESIII accumulated more data close to the $Y(4260)$ peak, which can be used to measure all the final states since the background level is very low as has been shown in the $\pi^+\pi^- J/\psi$ case,⁶³ but the real limiting factor is still the statistics. From the discussion in previous section, we know the production cross section of $e^+e^- \rightarrow \gamma X(3872)$ is at a few pb level, and the sample at BESIII has only about

10^4 produced $X(3872)$ events. This only allows measurement of final states with branching fractions at percent level.

5. The Y s: vector structures in e^+e^- annihilation

Among the charmonium-like states, there are many vectors with quantum numbers $J^{PC} = 1^{--}$ that are usually called Y states, like the $Y(4260)$,⁶⁹ the $Y(4360)$,^{70, 71} and the $Y(4660)$.⁷¹ The Y states show strong coupling to hidden-charm final states in contrast to the vector charmonium states in the same energy region ($\psi(4040)$, $\psi(4160)$, $\psi(4415)$) which couples dominantly to open-charm meson pairs.¹ These Y states are good candidates for new types of exotic particles and stimulated many theoretical interpretations, including tetraquarks, molecules, hybrids, or hadrocharmonia.⁶

These Y states were observed at B factories with limited statistics since they are produced from ISR processes with data collected at around 10.6 GeV in the bottomonium energy region^{20, 22, 26, 72} and the reconstruction efficiency is low. The high precision cross section measurements and the study of these states in different final states in direct e^+e^- annihilation in the charmonium energy region at BESIII experiment⁷ supply new insight into their nature.

5.1. $e^+e^- \rightarrow \pi^+\pi^- J/\psi$

The process $e^+e^- \rightarrow \pi^+\pi^- J/\psi$ at c.m. energies up to 5.0 GeV was first studied by the BaBar experiment, where the $Y(4260)$ was observed.⁶⁹ Belle measured the cross sections of $e^+e^- \rightarrow \pi^+\pi^- J/\psi$ at c.m. energies between 3.8 and 5.0 GeV and reported that $Y(4260)$ alone cannot describe the line shape satisfactorily.¹⁵ Improved measurements with both BaBar²⁶ and Belle²⁰ full data samples confirmed the existence of non- $Y(4260)$ component in $e^+e^- \rightarrow \pi^+\pi^- J/\psi$ but the line shape was parametrized with different models.

The cross sections of $e^+e^- \rightarrow \pi^+\pi^- J/\psi$ are measured precisely at c.m. energies from 3.77 to 4.60 GeV using 9 fb^{-1} of BESIII data.⁶⁸ The data sample used in this measurement includes the “XYZ data” and the “ R -scan data”. Figure 16 shows the measured cross sections, one can see clearly the $Y(4260)$ structure observed by BaBar and Belle experiments, but it is peaked at around 4.22 GeV rather than 4.26 GeV from the previous fits.^{20, 26}

Two resonant structures in the $Y(4260)$ peak region are needed in a fit to the cross sections. The first one has a mass of $(4222.0 \pm 3.1 \pm 1.4) \text{ MeV}/c^2$ and a width of $(44.1 \pm 4.3 \pm 2.0) \text{ MeV}$, while the second one has a mass of $(4320.0 \pm 10.4 \pm 7.0) \text{ MeV}/c^2$ and a width of $(101.4_{-19.7}^{+25.3} \pm 10.2) \text{ MeV}$. The mass of first resonance is lower than that of the $Y(4260)$ and it is much narrower. The second resonance is observed in $e^+e^- \rightarrow \pi^+\pi^- J/\psi$ for the first time, with a statistical significance larger than 7.6σ ,

28 Chang-Zheng Yuan

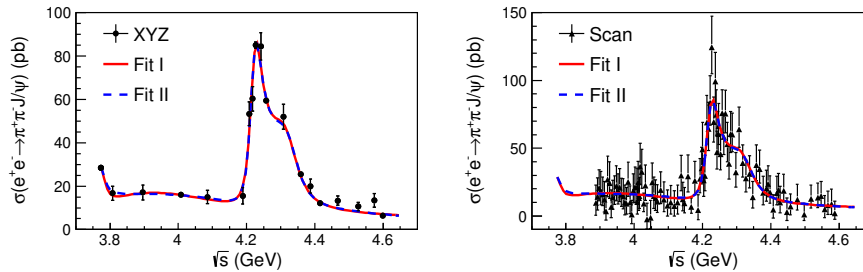


Fig. 16. Measured cross section $\sigma(e^+e^- \rightarrow \pi^+\pi^-J/\psi)$ and the simultaneous fit to the “XYZ data” (left) and “ R -scan data” (right) with the coherent sum of three BW functions (Fit I, red solid curves) and the coherent sum of an exponential continuum and two BW functions (Fit II, blue dashed curves). Dots with error bars are data.

it could be the $Y(4360)$ resonance observed in $e^+e^- \rightarrow \pi^+\pi^-\psi(2S)^{22,72}$ reported by the BaBar and Belle experiments.

It is worth pointing out that the lower mass structure (called $Y(4220)$ hereafter) is the main component of the $Y(4260)$ structure but with improved measurement of the resonant parameters thanks to the high luminosity data from BESIII. We will use $Y(4220)$ rather than $Y(4260)$ in the discussion below.

From the BESIII data, one can see that besides the $Y(4260)$ peak, the $\pi^+\pi^-J/\psi$ cross section is at 10–15 pb level, whether the cross section is due to pure continuum process or from the decays of other charmonium or charmonium-like states is still not clear. In fact, there are not many high luminosity data points in the $\psi(4040)$ and $\psi(4160)$ energy region, this prevents us from measuring the coupling of these states to $\pi^+\pi^-J/\psi$ mode, and the interference between these amplitudes and the $Y(4260)$ structures may affect the fit results significantly.

5.2. $e^+e^- \rightarrow \pi^+\pi^-h_c$

In 2013, BESIII reported the cross section measurement of $e^+e^- \rightarrow \pi^+\pi^-h_c$ at 13 c.m. energies from 3.9 to 4.4 GeV and found the magnitude of the cross sections is at the same order as that of $e^+e^- \rightarrow \pi^+\pi^-J/\psi$ but with a different line shape.⁷³ In this study, the h_c is reconstructed via its electric-dipole transition $h_c \rightarrow \gamma\eta_c$ with η_c to 16 exclusive hadronic final states.

Although no quantitative results were given in interpreting the $\pi^+\pi^-h_c$ line shape, the resonant structure at around 4.22 GeV/ c^2 is obvious.⁷³ A combined fit to the BESIII data together with the CLEO-c measurement at 4.17 GeV⁷⁴ results in a resonant structure with a mass of (4216 ± 18) MeV/ c^2 and a width of (39 ± 32) MeV,⁷⁵ different from any of the known Y and excited ψ states in this mass region at that time¹ but in agreement with the evidence of the structure observed in $e^+e^- \rightarrow \omega\chi_{c0}$.⁷⁶

In 2017, BESIII presented a follow-up study of $e^+e^- \rightarrow \pi^+\pi^-h_c$ at c.m. energies from 3.9 to 4.6 GeV using the “XYZ data” and the “ R -scan data” as used in $\pi^+\pi^-J/\psi$ analysis.⁴⁶ The cross sections are shown in Fig. 17 with dots and squares for R -scan and XYZ data samples, respectively. The measurements indicate that the cross section does decrease as c.m. energy increases to 4.6 GeV, and there are two resonant structures in the full energy range.

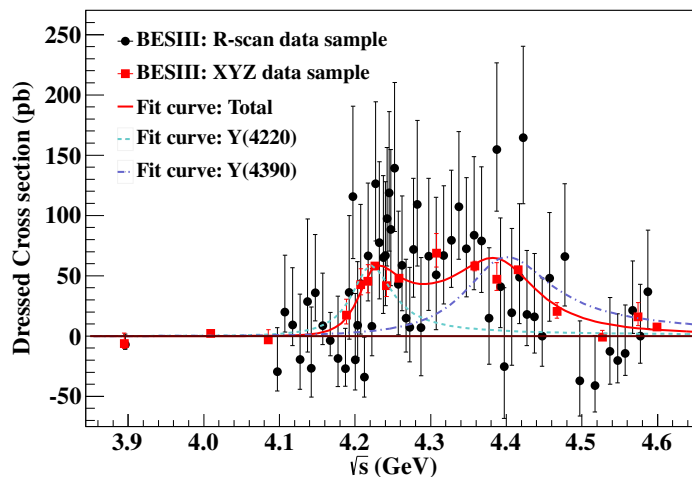


Fig. 17. Fit to the cross section of $e^+e^- \rightarrow \pi^+\pi^-h_c$ with the coherent sum of two BW functions (solid curve). The dash (dash-dot) curve shows the contribution from the two structures $Y(4220)$ ($Y(4390)$). The dots with error bars are the cross sections for R -scan data sample, the squares with error bars are the cross sections for XYZ data sample. Here the error bars are statistical uncertainty only.

Assuming the $\pi^+\pi^-h_c$ events come from two resonances, BESIII obtains $M = (4218.4_{-4.5}^{+5.5} \pm 0.9)$ MeV/ c^2 , $\Gamma = (66.0_{-8.3}^{+12.3} \pm 0.4)$ MeV, and the product of the electronic partial width and the decay branching fraction to $\pi^+\pi^-h_c$ $\Gamma_{e^+e^-}\mathcal{B}(Y(4220) \rightarrow \pi^+\pi^-h_c) = (4.6_{-1.4}^{+2.9} \pm 0.8)$ eV for $Y(4220)$, and $M = (4391.5_{-6.8}^{+6.3} \pm 1.0)$ MeV/ c^2 , $\Gamma = (139.5_{-20.6}^{+16.2} \pm 0.6)$ MeV, and $\Gamma_{e^+e^-}\mathcal{B}(Y(4390) \rightarrow \pi^+\pi^-h_c) = (11.6_{-4.4}^{+5.0} \pm 1.9)$ eV for $Y(4390)$, with a relative phase of $\phi = (3.1_{-0.9}^{+0.7} \pm 0.2)$ rad. The parameters of the low mass structure are consistent with those of the resonance observed in $e^+e^- \rightarrow \omega\chi_{c0}$ ⁷⁶ and in $e^+e^- \rightarrow \pi^+\pi^-J/\psi$ ⁶⁸ (see also Sec. 5.1). The high mass structure is different from the $Y(4360)$ ^{22,72} and $\psi(4415)$.¹

5.3. $e^+e^- \rightarrow \pi^+\pi^-\psi(2S)$

The BaBar experiment reported the update of the study of $e^+e^- \rightarrow \pi^+\pi^-\psi(2S)$ with ISR events⁷² with the full data sample recorded at and near the $\Upsilon(nS)$ ($n=2, 3, 4$) resonances and corresponds to an integrated luminosity of 520 fb⁻¹.

The cross sections for $e^+e^- \rightarrow \pi^+\pi^-\psi(2S)$ from 3.95 to 5.95 GeV are measured. A fit to the $\pi^+\pi^-\psi(2S)$ mass distribution yields a mass of $(4340 \pm 16 \pm 9)$ MeV/ c^2 and a width of $(94 \pm 32 \pm 13)$ MeV for the $Y(4360)$, and a mass of $(4669 \pm 21 \pm 3)$ MeV/ c^2 and a width of $(104 \pm 48 \pm 10)$ MeV for the $Y(4660)$.⁷² The results are in good agreement with the Belle measurement and confirm the $Y(4660)$ observed by the Belle experiment.⁷¹

Using the 980 fb^{-1} full data sample, Belle also updated the analysis of $e^+e^- \rightarrow \pi^+\pi^-\psi(2S)$ with ISR events.²² Fitting the mass spectrum of $\pi^+\pi^-\psi(2S)$ with two coherent BW functions (see Fig. 18 (left)), Belle obtains $M[Y(4360)] = (4347 \pm 6 \pm 3)$ MeV/ c^2 , $\Gamma[Y(4360)] = (103 \pm 9 \pm 5)$ MeV, $M[Y(4660)] = (4652 \pm 10 \pm 8)$ MeV/ c^2 and $\Gamma[Y(4660)] = (68 \pm 11 \pm 1)$ MeV.

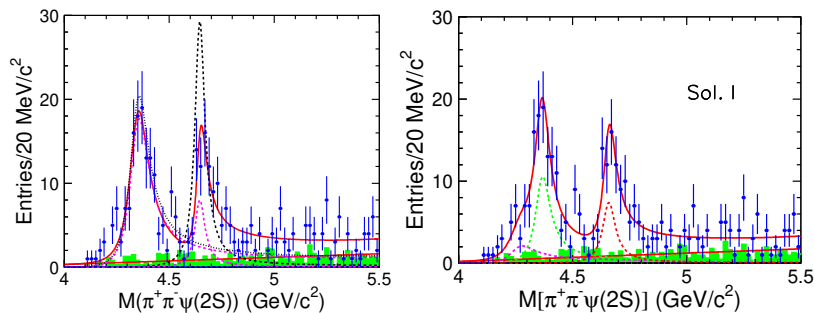


Fig. 18. The $\pi^+\pi^-\psi(2S)$ invariant mass distribution from the Belle experiment and the fit results with the coherent sum of two BW functions (left panel) and with the coherent sum of three BW functions (right panel). The points with error bars are data while the shaded histograms the normalized $\psi(2S)$ sideband backgrounds. The curves show the best fit and the dashed curves, show the contributions from different BW components.

Since there are some events accumulating at the mass region of the $Y(4260)$, the fit with the $Y(4260)$ included is also performed. In the fit, the mass and width of the $Y(4260)$ are fixed to the latest measured values at Belle.²⁰ The signal significance of the $Y(4260)$ is found to be 2.4σ . The fit results are shown in Fig. 18 (right) for one of the solutions. In this fit, one obtains $M[Y(4360)] = (4365 \pm 7 \pm 4)$ MeV/ c^2 , $\Gamma[Y(4360)] = (74 \pm 14 \pm 4)$ MeV, $M[Y(4660)] = (4660 \pm 9 \pm 12)$ MeV/ c^2 , and $\Gamma[Y(4660)] = (74 \pm 12 \pm 4)$ MeV. We can find that the resonant parameters depends on whether there is an additional $Y(4260)$ strongly.

BESIII measures $e^+e^- \rightarrow \pi^+\pi^-\psi(2S)$ using 5.1 fb^{-1} of data collected at 16 c.m. energies from 4.0 to 4.6 GeV²³ with two decay modes $\psi(2S) \rightarrow \pi^+\pi^-J/\psi$ and $\psi(2S) \rightarrow \text{neutrals} + J/\psi$, where “neutrals” refers to $\pi^0\pi^0$, π^0 , η , and $\gamma\gamma$. The measurement is almost background free, and BESIII measures the cross sections in good consistency with previous BaBar and Belle results,^{22,72} but with much improved precision, as shown in Fig. 19.

As the BESIII data can only reach 4.6 GeV, the parameters of the $Y(4660)$ are fixed to Belle measurement²² in the fit to the $e^+e^- \rightarrow \pi^+\pi^-\psi(2S)$ cross sections

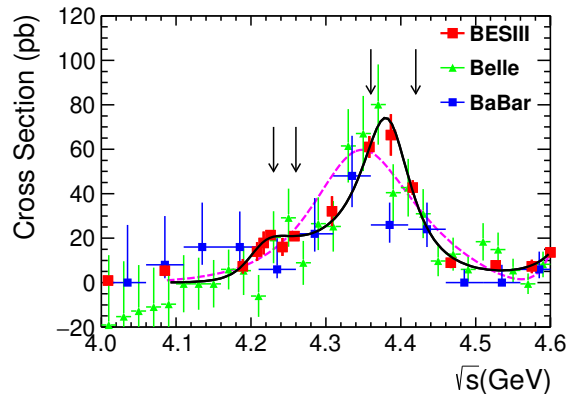


Fig. 19. Cross sections of $e^+e^- \rightarrow \pi^+\pi^-\psi(2S)$. The dots (red) are the BESIII results, the triangles (green) and squares (blue) are Belle and BaBar’s results, respectively. The solid curve is the fit to BESIII measurements with the coherent sum of three BW functions. The dashed curve (pink) is the fit to BESIII measurements with the coherent sum of two BW functions without the $Y(4220)$. The arrows mark the locations of four energy points with large integrated luminosities.

with the coherent sum of three BW amplitudes. The data require a lower-mass resonance with a mass $M = (4209.5 \pm 7.4 \pm 1.4) \text{ MeV}/c^2$ and a width $\Gamma = (80.1 \pm 24.6 \pm 2.9) \text{ MeV}$ with a statistical significance of 5.8σ , this is the first observation of the new decay mode $Y(4220) \rightarrow \pi^+\pi^-\psi(2S)$. The fit also results in a mass $M = (4383.8 \pm 4.2 \pm 0.8) \text{ MeV}/c^2$ and width $\Gamma = (84.2 \pm 12.5 \pm 2.1) \text{ MeV}$, for the $Y(4360)$. The fit results are also presented in Fig. 19.

5.4. $e^+e^- \rightarrow D^0D^{*-}\pi^+ + c.c.$

The cross section of $e^+e^- \rightarrow D^0D^{*-}\pi^+ + c.c.$ was first measured by the Belle experiment using ISR method.⁷⁷ No evidence for the $Y(4260)$, $Y(4360)$, $\psi(4415)$, $Y(4630)$, or $Y(4660)$ was found with limited statistics. BESIII reported improved measurements of the production cross section of $e^+e^- \rightarrow D^0D^{*-}\pi^+ + c.c.$ at c.m. energies from 4.05 to 4.60 GeV at 15 “XYZ data” points and 69 “R-scan data” points.⁷⁸ The D^0 meson is reconstructed in the $D^0 \rightarrow K^-\pi^+$ decay channel. The bachelor π^+ is also reconstructed, while the D^{*-} is inferred from energy-momentum conservation.

The measured cross sections are shown in Fig. 20, which is a significant improvement over the Belle measurement.⁷⁷ Two resonant structures around 4.23 and 4.40 GeV/c^2 are observed, in good agreement with the $Y(4260)$ and $Y(4390)$ observed in $e^+e^- \rightarrow \pi^+\pi^-h_c$.⁴⁶

A fit to the cross section is performed to determine the parameters of the resonant structures. The total amplitude is described by the coherent sum of a direct three-body phase-space term for $e^+e^- \rightarrow D^0D^{*-}\pi^+ + c.c.$ and two

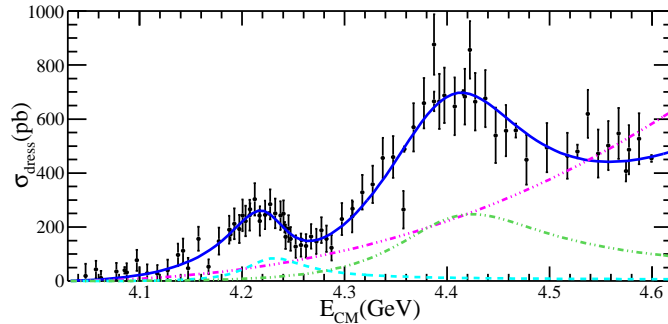


Fig. 20. Fit to the cross sections of $e^+e^- \rightarrow D^0 D^{*-} \pi^+ + c.c.$ from BESIII measurement. Dots with error bars are the data and the solid line is the total fit. The other lines show the contribution from each component.

BW functions, representing the two resonant structures. The fit yields a mass of $(4228.6 \pm 4.1 \pm 6.3)$ MeV/ c^2 and a width of $(77.0 \pm 6.8 \pm 6.3)$ MeV for the lower mass structure, and a mass of (4404.7 ± 7.4) MeV/ c^2 and a width of (191.9 ± 13.0) MeV for the higher mass one, where the errors are statistical only for the higher mass structure. Since the lower mass resonance is in good agreement as the $Y(4220)$ observed in $\pi^+\pi^- J/\psi$ and $\pi^+\pi^- h_c$ modes,^{46,68} this indicates the first observation of the $Y(4220)$ decays into open-charm final state $D^0 D^{*-} \pi^+ + c.c.$

The identification of the higher mass resonance is not straightforward. As there are known states $Y(4360)$ and $\psi(4415)$ in this energy region, it is hard to tell whether all the events come from a new $Y(4390)$ resonance. The above BESIII fit neglected possible contributions from known resonances and the complicated intermediate states in the three-body $D^0 D^{*-} \pi^+ + c.c.$ system. As an example, there must be contribution from $\psi(4415) \rightarrow \bar{D} D_2^*(2460) + c.c.$ in the high mass peak. Belle observed this process in $D\bar{D}\pi$ final state⁷⁹ and $D_2^*(2460)$ decays into $D^*\pi$ and $D\pi$ with similar rates. So the $\psi(4415)$ contribution in $e^+e^- \rightarrow D^0 D^{*-} \pi^+ + c.c.$ process must be taken into account in understanding the high mass structure.

The peak cross section of the $Y(4220)$ to this mode (consider also charge conjugate and isospin partner final states) is much higher than those final states with charmonium states, this suggests stronger coupling to open charm final state than to charmonium final state. The couplings of this state to other open charm final states should also be further measured to understand the decay dynamics.

5.5. $e^+e^- \rightarrow \omega\chi_{cJ}$ and $\phi\chi_{cJ}$

The possible strong coupling of the $Y(4260)$ to $\omega\chi_{cJ}$ final state was proposed by a few authors,^{80,81} the search for $e^+e^- \rightarrow \omega\chi_{cJ}$ are performed with the BESIII data above 4.2 GeV.^{76,82} The $\phi\chi_{cJ}$ thresholds are above 4.43 GeV, the study is only possible recently with BESIII data at c.m. energy 4.6 GeV.⁸³

The process $e^+e^- \rightarrow \omega\chi_{c0}$ is observed at $\sqrt{s} = 4.23$ and 4.26 GeV for the first

time⁷⁶ using χ_{c0} decays into a pair of $\pi^+\pi^-$ or K^+K^- (the decay rate of $\chi_{c0} \rightarrow \gamma J/\psi$ is small and other hadronic decay modes suffer from large background from $e^+e^- \rightarrow$ light hadrons), and the Born cross sections are measured to be $(55.4 \pm 6.0 \pm 5.9)$ and $(23.7 \pm 5.3 \pm 3.5)$ pb, respectively, which are comparable to those of $\pi^+\pi^- J/\psi$ process.⁶⁸ For other energy points, no significant signals are found, and the upper limits on the cross section at the 90% C.L. are determined.⁸² The cross sections are shown in Fig. 21, where a clear peaking structure close to the threshold is observed although there are only two statistically significant measurements available.

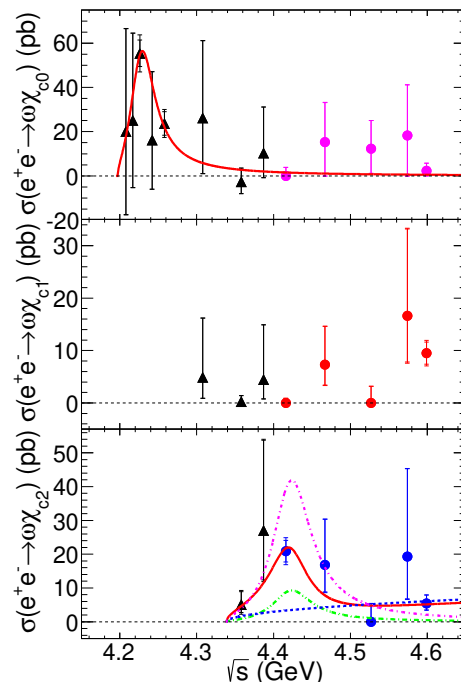


Fig. 21. Measured Born cross section for $e^+e^- \rightarrow \omega\chi_{cJ}$ ($J=0, 1, 2$) as a function of c.m. energy. From top to bottom are $e^+e^- \rightarrow \omega\chi_{c0}$, $\omega\chi_{c1}$, and $\omega\chi_{c2}$, respectively. The smaller error bars are statistical and the larger error bars are the combined statistical and systematic errors. The solid curves show the fit results.

The processes $e^+e^- \rightarrow \omega\chi_{c1,2}$ are observed for the first time at high energies.⁸² Here the $\chi_{c1,2}$ are reconstructed via their $\gamma J/\psi$ decays. A significant $\omega\chi_{c2}$ signal is found at $\sqrt{s}=4.42$ GeV, and the cross section is measured to be $(20.9 \pm 3.2 \pm 2.5)$ pb; while at $\sqrt{s}=4.6$ GeV, a clear $\omega\chi_{c1}$ signal is observed, and the cross section is measured to be $(9.5 \pm 2.1 \pm 1.3)$ pb. Due to low luminosity or low cross section at other energies, no significant signals are observed.

The data reveal a sizable $\omega\chi_{c0}$ production at around $4.23 \text{ GeV}/c^2$, as predicted

in Ref. 81. By assuming the $\omega\chi_{c0}$ signals come from a single resonance, the cross section of $e^+e^- \rightarrow \omega\chi_{c0}$ are fitted with a BW function, and the mass is $(4226 \pm 8 \pm 6)$ MeV/ c^2 , and width is $(39 \pm 12 \pm 2)$ MeV (shown in Fig. 21). The parameters are consistent with those of the narrow structure in the $e^+e^- \rightarrow \pi^+\pi^-h_c$,^{46,75} $\pi^+\pi^-J/\psi$,⁶⁸ $D^0D^{*-}\pi^+ + c.c.$,⁷⁸ and $\pi^+\pi^-\psi(2S)$ ²³ processes. In fact, it is in the $e^+e^- \rightarrow \omega\chi_{c0}$ mode that the $Y(4220)$ (or $Y(4230)$) structure was first reported.⁷⁶ In $e^+e^- \rightarrow \omega\chi_{c2}$, the cross section is higher at around 4.416 GeV than at other energies, this may suggest $\psi(4415) \rightarrow \omega\chi_{c2}$ decays but more measurements in the vicinity of the $\psi(4415)$ peak are needed.

BESIII searches for the production of $e^+e^- \rightarrow \phi\chi_{cJ}$ with data sample at c.m. energy of 4.6 GeV.⁸³ The processes $e^+e^- \rightarrow \phi\chi_{c1}$ and $\phi\chi_{c2}$ are observed for the first time, each with a statistical significance of more than 10σ , and the Born cross sections are measured to be $(4.2_{-1.0}^{+1.7} \pm 0.3)$ and $(6.7_{-1.7}^{+3.4} \pm 0.5)$ pb, respectively. No significant signals are observed for $e^+e^- \rightarrow \phi\chi_{c0}$ and upper limit on the Born cross section is estimated to be 5.4 pb at the 90% C.L.

5.6. $e^+e^- \rightarrow \eta h_c$

The process $e^+e^- \rightarrow \eta h_c$ are searched for at c.m. energies from 4.085 to 4.600 GeV at BESIII.⁸⁴ Clear signals of $e^+e^- \rightarrow \eta h_c$ are observed at $\sqrt{s} = 4.226$ GeV for the first time, 41 ± 9 signal events with a statistical significance of 5.8σ are observed, and the Born cross section is measured to be $(9.5_{-2.0}^{+2.2} \pm 2.7)$ pb. Evidence for the signal process at $\sqrt{s} = 4.358$ GeV is also observed, there are 19 ± 6 signal events and the statistical significance is 4.3σ , the cross section is measured to be $(10.0_{-2.7}^{+3.1} \pm 2.6)$ pb. For the other c.m. energies considered, no significant signals are found, and upper limits on the cross section at the 90% C.L. are determined.

Comparing with the cross section of $e^+e^- \rightarrow \pi^+\pi^-h_c$,²¹ which is shown in Fig. 22, one finds that the cross section at $\sqrt{s} = 4.226$ GeV is larger than that at $\sqrt{s} = 4.258$ GeV in both processes. This may suggest $e^+e^- \rightarrow \eta h_c$ have similar line shape as $e^+e^- \rightarrow \pi^+\pi^-h_c$ ⁴⁶ or there is $Y(4220) \rightarrow \eta h_c$ transition. However, due to the limited statistics, one cannot draw a solid conclusion about the production mechanism of $e^+e^- \rightarrow \eta h_c$.

5.7. $e^+e^- \rightarrow \eta J/\psi$ and $\eta' J/\psi$

Using data samples at c.m. energies of 3.81–4.60 GeV, BESIII measures the Born cross sections of $e^+e^- \rightarrow \eta J/\psi$ ^{85,86} as shown in Fig. 23. Good agreement with the previous Belle measurements⁸⁷ is observed. As Belle measures the cross section with ISR data, there are more data points but the errors are large due to low statistics, the BESIII measurements have better precision, however, are only available at a few data points.

The process $e^+e^- \rightarrow \eta' J/\psi$ is investigated at 14 c.m. energies from 4.1 to 4.6 GeV.⁸⁸ Significant $e^+e^- \rightarrow \eta' J/\psi$ signals are observed at $\sqrt{s} = 4.226$ and

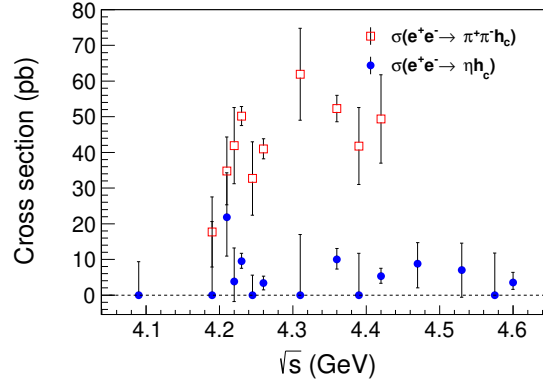


Fig. 22. Comparison between the cross sections of $e^+e^- \rightarrow \eta h_c$ (dots with error bars) and $e^+e^- \rightarrow \pi^+\pi^- h_c$ (squares with error bars).²¹ The errors are statistical only.

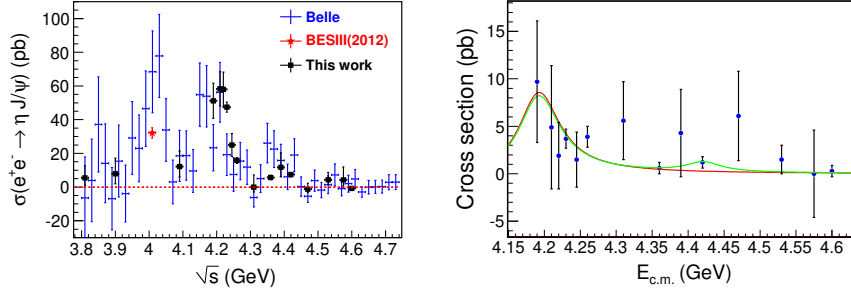


Fig. 23. (Left panel) Born cross sections of $e^+e^- \rightarrow \eta J/\psi$ from BESIII^{85,86} (black dots and the red star) and Belle experiments⁸⁷ (blue dots). (Right panel) Born cross sections of $e^+e^- \rightarrow \eta' J/\psi$ from BESIII⁸⁸ (dots with error bars), and the fit with a $\psi(4160)$ resonance (red curve), or with a combination of $\psi(4160)$ and $\psi(4415)$ resonances (green curve).

4.258 GeV for the first time, and the corresponding Born cross sections are measured to be $(3.7 \pm 0.7 \pm 0.3)$ and $(3.9 \pm 0.8 \pm 0.3)$ pb, respectively. The upper limits of Born cross sections at the 90% C.L. are set for the other 12 c.m. energy points where no significant signal is observed. The results are shown in the right panel of Fig. 23.

Compared with the Born cross section of $e^+e^- \rightarrow \eta J/\psi$, the cross section of $e^+e^- \rightarrow \eta' J/\psi$ is much smaller. BESIII have collected lots of data at a few data points around 4.2 GeV but the cross sections are not reported. With these new data, we may have a better feeling about the line shapes of these two modes, especially around the $\psi(4160)$ – $Y(4220)$ mass region. More data points around 4.0 GeV will be helpful to understand the first peak observed by Belle in $e^+e^- \rightarrow \eta J/\psi$ mode, further data around 4.4 GeV will enable a check if the small peak observed in both Belle and BESIII data in $e^+e^- \rightarrow \eta J/\psi$ mode is statistical fluctuation or from $Y(4360)$ or $\psi(4415)$ decays.

5.8. Efforts in extracting resonant parameters from combined fits

As the cross sections of different final states have some common features, and some of the final states have been measured by different experiments, these data are used to do combined fit to extract more information about the resonant structures.^{89,90}

In Ref. 89, the authors use the measured cross sections of $e^+e^- \rightarrow \omega\chi_{c0}$,⁸² $\pi^+\pi^-h_c$,⁴⁶ $\pi^+\pi^-J/\psi$,⁶⁸ and $D^0D^{*-}\pi^+ + c.c.$ ⁷⁸ processes by BESIII experiment only to measure the resonant parameters of the $Y(4220)$.

The cross sections are parametrized as the coherent sum of a few amplitudes, either resonance represented by a BW function or non-resonant term parametrized with a phase space distribution. In fitting to the data shown in Fig. 24, the $Y(4220)$ is assumed to be in all the modes while the other resonances may appear in one or more modes. The fit determines the mass of the $Y(4220)$ as $(4219.6 \pm 3.3 \pm 5.1)$ MeV/ c^2 and the width is $(56.0 \pm 3.6 \pm 6.9)$ MeV. It is noticed that the mass of the $Y(4220)$ is very close to the threshold of $D_s^*\bar{D}_s^*$ threshold (4224 MeV/ c^2),¹ the possibility of its coupling to charmed strange meson pairs (as well as charmed non-strange meson pairs) should be studied.

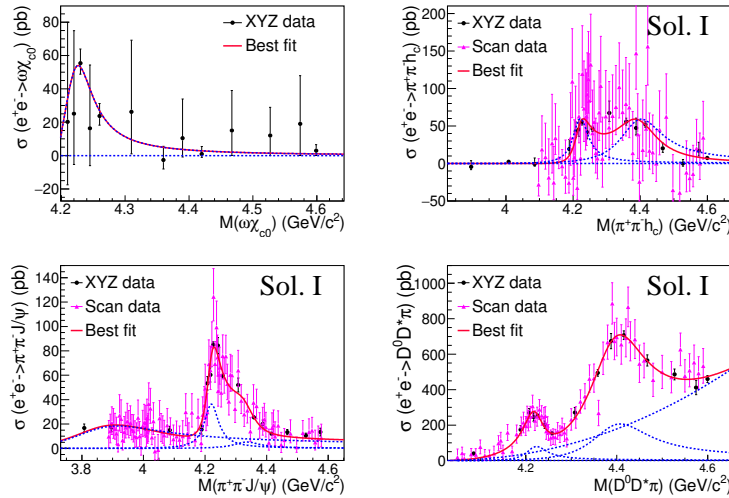


Fig. 24. The combined fit to $e^+e^- \rightarrow \omega\chi_{c0}$ (top left), $\pi^+\pi^-h_c$ (top right), $\pi^+\pi^-J/\psi$ (bottom left), and $D^0D^{*-}\pi^+ + c.c.$ (bottom right).⁸⁹ The dots and the triangles with error bars are data. The solid curves are the projections from the best fit. The dashed curves show the fitted resonance components. Only one solution of the fit is presented here.

The fit also measures the product of the leptonic decay width and the decay branching fraction to a final state. By considering the isospin symmetric modes of the measured channels, the lower limit on the leptonic partial width of the $Y(4220)$ is estimated to be $\Gamma_{e^+e^-} > (29.1 \pm 2.5 \pm 7.0)$ eV, where the first errors are from fit and the second errors are the systematic errors with the uncertainties from different

fit scenarios. This lower limit on the leptonic partial width of the $Y(4220)$ is close to the prediction from LQCD for a hybrid vector charmonium state.⁹¹

In Ref. 90, more modes are included in the combined fit, and the resonant parameters of the $Y(4390)$ and $Y(4660)$ are also measured with some assumptions.

All these fits parametrize the amplitude as the coherent sum of BW functions with constant widths. These assumptions may introduce bias since some of the states are wide and overlap with each other. As the states decay also into open charm final states with thresholds not very far from the resonant peak, the width must be energy dependent.

A coupled-channel approach is tried to perform a simultaneous fit to the open-charm data measured by Belle in 3.7–4.7 GeV energy region.⁹² In principle, this can be extended to all the channels to have a better understanding of the line shapes observed. Although there are still lots of technical problems to be solved, this is a right trend to understand the vector states produced in e^+e^- annihilation. BESIII measurements on the open-charm cross sections are obviously very important, more data points in the measurements of the final states with charmonium are also necessary.

6. Observation of $\psi(1^3D_2)$

BESIII observed $X(3823)$ in the $e^+e^- \rightarrow \pi^+\pi^-X(3823) \rightarrow \pi^+\pi^-\gamma\chi_{c1}$ with a statistical significance of 6.2σ in data samples at c.m. energies of 4.23, 4.26, 4.36, 4.42, and 4.60 GeV.⁹³

Figure 25 shows the fitted results to $\pi^+\pi^-$ recoil mass distributions for events in the χ_{c1} and χ_{c2} signal regions. The fit yields 19 ± 5 $X(3823)$ signal events in the $\gamma\chi_{c1}$ mode, with a measured mass of $X(3823)$ of $(3821.7 \pm 1.3 \pm 0.7)$ MeV/ c^2 . For the $\gamma\chi_{c2}$ mode, no significant $X(3823)$ signal is observed, and an upper limit on its production rate is determined. The upper limit on the intrinsic width of $X(3823)$ is determined as $\Gamma[X(3823)] < 16$ MeV at the 90% C.L. This measurement agrees with the values found by Belle.⁹⁴

The production cross sections $\sigma^B(e^+e^- \rightarrow \pi^+\pi^-X(3823)) \cdot \mathcal{B}(X(3823) \rightarrow \gamma\chi_{c1}, \gamma\chi_{c2})$ are also measured at these c.m. energies. The cross sections of $e^+e^- \rightarrow \pi^+\pi^-X(3823)$ are fitted with the $Y(4360)$ shape or the $\psi(4415)$ shape, with their resonance parameters fixed to the PDG values.¹ Figure 26 shows the fitted results, we can see that both the $Y(4360)$ and $\psi(4415)$ describe the data well.

The $X(3823)$ resonance is a good candidate for the $\psi(1^3D_2)$ charmonium state. According to potential models,⁹⁵ the D -wave charmonium states are expected to be within a mass range of 3.82–3.85 GeV/ c^2 . Among these, the $1^1D_2 \rightarrow \gamma\chi_{c1}$ transition is forbidden because of C -parity conservation, and the amplitude for $1^3D_3 \rightarrow \gamma\chi_{c1}$ is expected to be small.⁹⁶ The mass of $\psi(1^3D_2)$ is in the 3.810 ~ 3.840 GeV/ c^2 range predicted by several phenomenological calculations.⁹⁷ In this

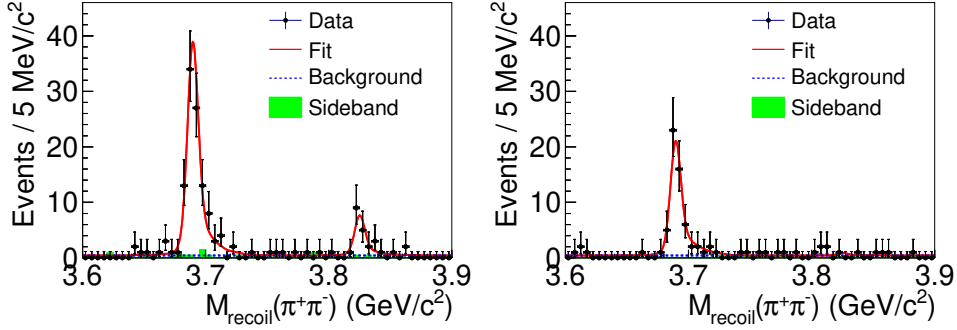


Fig. 25. Simultaneous fit to the $M_{\text{recoil}}(\pi^+\pi^-)$ distribution of $\gamma\chi_{c1}$ events (left) and $\gamma\chi_{c2}$ events (right), respectively. Dots with error bars are data, red solid curves are total fit, dashed blue curves are background, and the green shaded histograms are J/ψ mass sideband events.

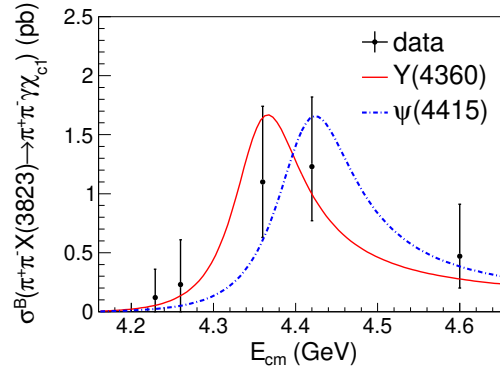


Fig. 26. Comparison of the energy-dependent cross sections of $\sigma^B[e^+e^- \rightarrow \pi^+\pi^-X(3823)] \cdot \mathcal{B}[X(3823) \rightarrow \gamma\chi_{c1}]$ to the $Y(4360)$ and $\psi(4415)$ line shapes. Dots with error bars are data. The red solid (blue dashed) curve shows a fit with the $Y(4360)$ ($\psi(4415)$) line shape.

case, the mass of $\psi(1^3D_2)$ is above the $D\bar{D}$ threshold but below the $D\bar{D}^*$ threshold. Because $\psi(1^3D_2) \rightarrow D\bar{D}$ violates parity, $\psi(1^3D_2)$ is expected to be narrow, in agreement with the observation, and $\psi(1^3D_2) \rightarrow \gamma\chi_{c1}$ is expected to be a dominant decay mode.^{97,98} From the cross section measurement, BESIII obtains the ratio $\frac{\mathcal{B}[X(3823) \rightarrow \gamma\chi_{c2}]}{\mathcal{B}[X(3823) \rightarrow \gamma\chi_{c1}]} < 0.42$ at the 90% C.L., which also agrees with expectations for the $\psi(1^3D_2)$ state.⁹⁸

7. The $Y(4140)$ and other states in $\phi J/\psi$ system

Using exclusive $B^+ \rightarrow J/\psi\phi K^+$ decays, CDF Collaboration observed a narrow structure near the $J/\psi\phi$ mass threshold with a statistical significance greater than 5σ .^{99,100} The mass and width of this structure are fitted to be $(4143.4_{-3.0}^{+2.9} \pm 0.6)$ MeV/ c^2 and $(15.3_{-6.1}^{+10.4} \pm 2.5)$ MeV, respectively. There were many experi-

mental studies in the earlier years, but very controversial results were reported, as described in Ref. 101.

BESIII searches for $Y(4140)$ via $e^+e^- \rightarrow \gamma\phi J/\psi$ at $\sqrt{s} = 4.23, 4.26, 4.36,$ and 4.60 GeV, but no significant $Y(4140)$ signal is observed in any of the data samples.^{83,102} The upper limits of the product of the cross section and branching fraction $\sigma[e^+e^- \rightarrow \gamma Y(4140)] \cdot \mathcal{B}(Y(4140) \rightarrow \phi J/\psi)$ are determined to be 0.35, 0.28, 0.33, and 1.2 pb at $\sqrt{s} = 4.23, 4.26, 4.36,$ and 4.60 GeV, respectively, at the 90% C.L.

With 3 fb^{-1} data collected at c.m. energies 7 and 8 TeV, LHCb reconstructed $4289 \pm 151 B^+ \rightarrow J/\psi\phi K^+$ decays,¹⁰³ this data sample makes the amplitude analysis in the 6D phase space composed of invariant masses and decay angles possible, and offers the best sensitivity to study the resonant structures in $\phi J/\psi$ system. The data requires not only two $J^{PC} = 1^{++}$ states, the $Y(4140)$ and $Y(4274)$,¹⁰⁰ but also two new $J^{PC} = 0^{++}$ states, $X(4500)$ and $X(4700)$. The fit results are shown in Fig. 27 and listed in Table 3. Confirmation from other experiments and further experimental investigation of them are needed.

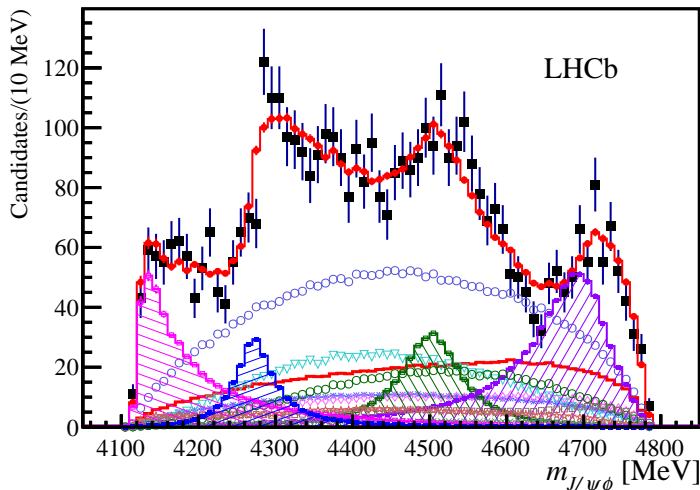


Fig. 27. Distributions of $\phi J/\psi$ invariant masses for the $B^+ \rightarrow J/\psi\phi K^+$ candidates (black data points) compared with the fit containing eight $K^{*+} \rightarrow \phi K^+$ and five $X \rightarrow J/\psi\phi$ contributions. The total fit is given by the red points with error bars. Individual fit components are also shown.

8. Summary and Perspectives

With the large data samples available at LHCb and BESIII experiments, we achieved a lot in the study of the exotic states in the charmed sector: new charged charmonium-like states $Z_c(3900)$ and $Z_c(4020)$ are discovered; the spin-parity quan-

Table 3. Results for significances, masses, and widths of the $\phi J/\psi$ components in $B^+ \rightarrow J/\psi \phi K^+$ from LHCb experiment.

States	Significance	J^{PC}	Mass (MeV/ c^2)	Width (MeV)
$Y(4140)$	8.4σ	1^{++}	$4146.5 \pm 4.5^{+4.6}_{-2.8}$	$83 \pm 21^{+21}_{-14}$
$Y(4274)$	6.0σ	1^{++}	$4273.3 \pm 8.3^{+17.2}_{-3.6}$	$56 \pm 11^{+8}_{-11}$
$X(4500)$	6.1σ	0^{++}	$4506 \pm 11^{+12}_{-15}$	$92 \pm 21^{+21}_{-20}$
$X(4700)$	5.6σ	0^{++}	$4704 \pm 10^{+14}_{-24}$	$120 \pm 31^{+42}_{-33}$

tum numbers of the $X(3872)$, $Z_c(3900)$, and $Z_c(4430)$ are determined; and the $Y(4260)$ structure is found to be dominated by the $Y(4220)$ with lower mass, narrower width, and more decay modes; and so on. However, there are still a lot to learn with the existing and the coming data samples to understand these states better:

- In the X sector:
 - Search for more decay modes (including confirmation of $X(3872) \rightarrow \gamma\psi(2S)$) and measure the absolute branching fraction of $X(3872)$ decays.
 - Measure the production cross section of $e^+e^- \rightarrow \gamma X(3872)$ and $\pi^+\pi^-\psi(1^3D_2)$, determine whether they are from resonance decays or continuum production.
 - Study of the other X states, such as $X(3915)$ and $X(4140)$ ($Y(4140)$), in e^+e^- annihilation and B decays.
- In the Y sector:
 - Measure more precisely the line shapes of more final states in e^+e^- annihilation, including open-charm and charmonium final states.
 - Try coupled-channel analysis with more information.
 - Search for the Y states in B or other particle decays.
- In the Z sector:
 - Measure the Z_c production cross section in e^+e^- annihilation, determine whether they are produced from resonance decays or continuum production.
 - Search for Z_c production in B or other particle decays.
 - Determine the quantum numbers, measure the Argand plot of the resonant amplitude, and search for more decay modes.
 - Search for Z_{cs} state decaying into $K^\pm J/\psi$, $D_s^- D^{*0} + c.c.$, or $D_s^{*-} D^0 + c.c.$
 - Search for more Z_c states.

As we have mentioned in previous sections, besides the 3 fb^{-1} data at 7 and 8 TeV used in most of the LHCb analyses, there are 4 fb^{-1} data at 13 TeV and will

reach 5 fb^{-1} by the end of 2018. These data will allow much improved analyses of many topics discussed above such as the $X(3872)$ decay properties and the searches for the Y and $Z_c(3900)$ states in B decays.

BESIII has achieved a lot in the study of the XYZ states and the conventional charmonium states. However, there are still some data (see Table 1) not analyzed and data at more energy points will be taken.¹⁰⁴ More analyses with these data samples will allow many improved understanding of the XYZ states, especially the $X(3872)$, $Y(4260)$, $Z_c(3900)$, and $Z_c(4020)$. BEPCII is upgrading the maximum c.m. energy from 4.6 to 4.9 GeV in two years, this will enable a full coverage of the $Y(4660)$ ⁷¹ and $Y(4630)$ ¹⁰⁵ resonances, improved measurements of their properties are expected.

Belle II⁵⁰ will start collecting data in 2019, and will accumulate 50 ab^{-1} data at the $\Upsilon(4S)$ peak by 2025. These data samples can be used to study the XYZ and charmonium states in many different ways,⁵ among which ISR can produce events in the same energy range covered by BESIII. Figure 28 shows the effective luminosity at BEPCII energy in the Belle II data samples. We can see that, 50 ab^{-1} Belle II data correspond to $2,000\text{--}2,800 \text{ pb}^{-1}$ data for every 10 MeV from 4–5 GeV, similar statistics will be reached for modes like $e^+e^- \rightarrow \pi^+\pi^-J/\psi$ at Belle II and BESIII taking into account the fact that Belle II has lower efficiency. Belle II has the advantage that data at different energies will be accumulated at the same time, making the analysis much simpler than at BESIII at many data points.

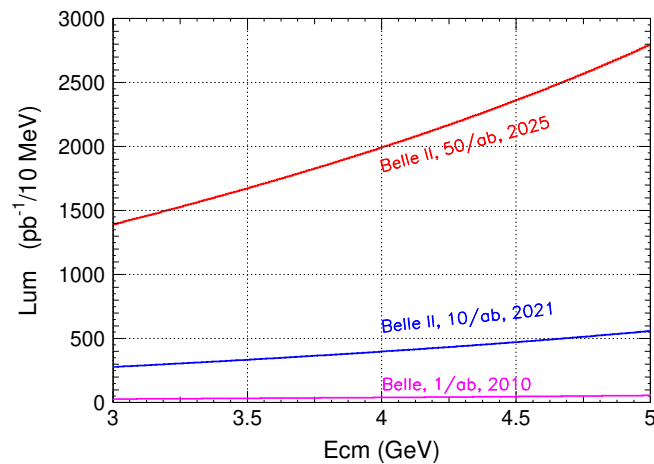


Fig. 28. Effective luminosity at low energy in the Belle and Belle II $\Upsilon(4S)$ data samples.

There are two super τ -charm factories proposed, the HIEPA in China¹⁰⁶ and the SCT in Russia.¹⁰⁷ Both machines run at c.m. energies of up to 5 GeV or higher and a peak luminosity of $10^{35} \text{ cm}^{-2}\text{s}^{-1}$ which is a factor of 100 improvement over the BEPCII. This enables a systematic study of the XYZ and charmonium states with unprecedented precision.

Acknowledgments

This work is supported in part by National Natural Science Foundation of China (NSFC) under contract Nos. 11235011, 11475187, and 11521505; the Ministry of Science and Technology of China under Contract No. 2015CB856701; Key Research Program of Frontier Sciences, CAS, Grant No. QYZDJ-SSW-SLH011; and the CAS Center for Excellence in Particle Physics (CCEPP).

References

1. C. Patrignani *et al.* [Particle Data Group], *Chin. Phys. C* **40**, 100001 (2016). M. Tanabashi *et al.* [Particle Data Group], *Phys. Rev. D* **98**, 030001 (2018).
2. For a review, see E. Klempt and A. Zaitsev, *Phys. Rept.* **454**, 1 (2007).
3. B. Aubert *et al.* [BaBar Collaboration], *Nucl. Instrum. Methods Phys. Res., Sect. A* **479**, 1 (2002).
4. A. Abashian *et al.*, *Nucl. Instrum. Methods Phys. Res., Sect. A* **479**, 117 (2002).
5. A. J. Bevan *et al.* [BaBar and Belle Collaborations], *Eur. Phys. J. C* **74**, 3026 (2014).
6. For recent reviews, see F. K. Guo, C. Hanhart, U. G. Meißner, Q. Wang, Q. Zhao and B. S. Zou, *Rev. Mod. Phys.* **90**, no. 1, 015004 (2018). H. X. Chen, W. Chen, X. Liu and S. L. Zhu, *Phys. Rept.* **639**, 1 (2016); N. Brambilla *et al.*, *Eur. Phys. J. C* **71**, 1534 (2011).
7. M. Ablikim *et al.* [BESIII Collaboration], *Nucl. Instrum. Methods Phys. Res., Sect. A* **614**, 345 (2010).
8. A. A. Alves, Jr. *et al.* [LHCb Collaboration], *JINST* **3**, S08005 (2008); R. Aaij *et al.* [LHCb Collaboration], *Int. J. Mod. Phys. A* **30**, 1530022 (2015).
9. Xin Li *et al.*, *Radiat. Detect. Technol. Methods.* **1**, 13 (2017); Ying-Xiao Guo *et al.*, *Radiat. Detect. Technol. Methods.* **1**, 15 (2017).
10. D. M. Asner *et al.*, *Int. J. Mod. Phys. A* **24**, S1 (2009).
11. M. Ablikim *et al.* [BESIII Collaboration], *Phys. Rev. Lett.* **110**, 252001 (2013).
12. M. Ablikim *et al.* [BESIII Collaboration], *Chin. Phys. C* **40**, 063001 (2016).
13. M. Ablikim *et al.* [BESIII Collaboration], *Chin. Phys. C* **39**, 093001 (2015).
14. M. Ablikim *et al.* [BESIII Collaboration], *Chin. Phys. C* **41**, 063001 (2017).
15. C. Z. Yuan *et al.* [Belle Collaboration], *Phys. Rev. Lett.* **99**, 182004 (2007).
16. Tomasz Skwarnicki, talk at “The 9th International Workshop on Charm Physics”, May 21 to 25, 2018, Novosibirsk, Russia. <https://indico.inp.nsk.su/event/10/session/2/contribution/77/material/slides/0.pdf>
17. S. K. Choi *et al.* [Belle Collaboration], *Phys. Rev. Lett.* **100**, 142001 (2008).
18. K. Chilikin *et al.* [Belle Collaboration], *Phys. Rev. D* **88**, 074026 (2013).
19. R. Aaij *et al.* [LHCb Collaboration], *Phys. Rev. Lett.* **112**, 222002 (2014).
20. Z. Q. Liu *et al.* [Belle Collaboration], *Phys. Rev. Lett.* **110**, 252002 (2013).
21. M. Ablikim *et al.* [BESIII Collaboration], *Phys. Rev. Lett.* **111**, 242001 (2013).
22. X. L. Wang *et al.* [Belle Collaboration], *Phys. Rev. D* **91**, 112007 (2015).

23. M. Ablikim *et al.* [BESIII Collaboration], Phys. Rev. D **96**, 032004 (2017).
24. R. Mizuk *et al.* [Belle Collaboration], Phys. Rev. D **78**, 072004 (2008).
25. K. Chilikin *et al.* [Belle Collaboration], Phys. Rev. D **90**, 112009 (2014).
26. J. P. Lees *et al.* [BaBar Collaboration], Phys. Rev. D **86**, 051102(R) (2012).
27. T. Xiao, S. Dobbs, A. Tomaradze and K. K. Seth, Phys. Lett. B **727**, 366 (2013).
28. M. Ablikim *et al.* [BESIII Collaboration], Phys. Rev. Lett. **110**, 252001 (2013).
29. M. Ablikim *et al.* [BESIII Collaboration], Phys. Rev. Lett. **112**, 022001 (2014).
30. M. Ablikim *et al.* [BESIII Collaboration], Phys. Rev. D **92**, 092006 (2015).
31. M. Ablikim *et al.* [BESIII Collaboration], Phys. Rev. Lett. **115**, 222002 (2015).
32. M. Ablikim *et al.* [BESIII Collaboration], Phys. Rev. Lett. **119**, 072001 (2017).
33. S. U. Chung, Phys. Rev. D **57**, 431 (1998); S. U. Chung, Phys. Rev. D **48**, 1225 (1993); S. U. Chung and J. M. Friedrich, Phys. Rev. D **78**, 074027 (2008).
34. Chang-Zheng Yuan, talk at “The 9th International Workshop on Charm Physics”, May 21 to 25, 2018, Novosibirsk, Russia. <https://indico.inp.nsk.su/event/10/session/2/contribution/41/material/slides/0.pdf>
35. A. Esposito, A. L. Guerrieri and A. Pilloni, Phys. Lett. B **746**, 194 (2015).
36. G. Li, X. H. Liu and Z. Zhou, Phys. Rev. D **90**, 054006 (2014).
37. H. W. Ke, Z. T. Wei and X. Q. Li, Eur. Phys. J. C **73**, 2561 (2013).
38. L. Ma, X. H. Liu, X. Liu and S. L. Zhu, Phys. Rev. D **91**, 034032 (2015).
39. L. Ma, W. Z. Deng, X. L. Chen and S. L. Zhu, arXiv:1512.01938 [hep-ph].
40. M. B. Voloshin, arXiv:1806.05651 [hep-ph].
41. M. Ablikim *et al.* [BESIII Collaboration], Phys. Rev. D **92**, 012008 (2015).
42. M. Ablikim *et al.* [BESIII Collaboration], Phys. Rev. D **92**, 032009 (2015).
43. M. Ablikim *et al.* [BESIII Collaboration], Phys. Rev. Lett. **113**, 212002 (2014).
44. M. Ablikim *et al.* [BESIII Collaboration], Phys. Rev. Lett. **112**, 132001 (2014).
45. M. Ablikim *et al.* [BESIII Collaboration], Phys. Rev. Lett. **115**, 182002 (2015).
46. M. Ablikim *et al.* [BESIII Collaboration], Phys. Rev. Lett. **118**, 092002 (2017).
47. B. Aubert *et al.* [BaBar Collaboration], Phys. Rev. D **79**, 112001 (2009).
48. A. Bondar, talk at “The 9th International Workshop on Charm Physics”, May 21 to 25, 2018, Novosibirsk, Russia. <https://indico.inp.nsk.su/event/10/session/2/contribution/74/material/slides/0.pdf>
49. A. Bondar *et al.* [Belle Collaboration], Phys. Rev. Lett. **108**, 122001 (2012); A. Garmash *et al.* [Belle Collaboration], Phys. Rev. Lett. **116**, 212001 (2016).
50. T. Abe *et al.* [Belle-II Collaboration], arXiv:1011.0352 [physics.ins-det].
51. An evidence for $Z_c(3900)$ production was reported very recently in V. M. Abazov *et al.* [D0 Collaboration], arXiv:1807.00183 [hep-ex].
52. S. K. Choi *et al.* [Belle Collaboration], Phys. Rev. Lett. **91**, 262001 (2003).
53. D. Acosta *et al.* [CDF Collaboration], Phys. Rev. Lett. **93**, 072001 (2004).
54. V. M. Abazov *et al.* [D0 Collaboration], Phys. Rev. Lett. **93**, 162002 (2004).
55. B. Aubert *et al.* [BaBar Collaboration], Phys. Rev. D **71**, 071103 (2005).
56. B. Aubert *et al.* [BaBar Collaboration], Phys. Rev. D **74**, 071101 (2006).
57. V. Bhardwaj *et al.* [Belle Collaboration], Phys. Rev. Lett. **107**, 091803 (2011).
58. R. Aaij *et al.* [LHCb Collaboration], Nucl. Phys. B **886**, 665 (2014).
59. A. Abulencia *et al.* [CDF Collaboration], Phys. Rev. Lett. **98**, 132002 (2007).
60. R. Aaij *et al.* [LHCb Collaboration], Phys. Rev. Lett. **110**, 222001 (2013).
61. A. Abulencia *et al.* [CDF Collaboration], Phys. Rev. Lett. **96**, 102002 (2006).
62. R. Aaij *et al.* [LHCb Collaboration], Phys. Rev. D **92**, 011102 (2015).
63. M. Ablikim *et al.* [BESIII Collaboration], Phys. Rev. Lett. **112**, 092001 (2014).
64. B. Aubert *et al.* [BaBar Collaboration], Phys. Rev. Lett. **102**, 132001 (2009).
65. B. Aubert *et al.* [BaBar Collaboration], Phys. Rev. Lett. **96**, 052002 (2006).

66. Y. Kato *et al.* [Belle Collaboration], Phys. Rev. D **97**, 012005 (2018).
67. C. Z. Yuan for the Belle Collaboration, arXiv:0910.3138 [hep-ex].
68. M. Ablikim *et al.* [BESIII Collaboration], Phys. Rev. Lett. **118**, 092001 (2017).
69. B. Aubert *et al.* [BaBar Collaboration], Phys. Rev. Lett. **95**, 142001 (2005).
70. B. Aubert *et al.* [BaBar Collaboration], Phys. Rev. Lett. **98**, 212001 (2007).
71. X. L. Wang *et al.* [Belle Collaboration], Phys. Rev. Lett. **99**, 142002 (2007).
72. J. P. Lees *et al.* [BaBar Collaboration], Phys. Rev. D **89**, 111103 (2014).
73. M. Ablikim *et al.* [BESIII Collaboration], Phys. Rev. Lett. **111**, 242001 (2013).
74. T. K. Pedlar *et al.* [CLEO Collaboration], Phys. Rev. Lett. **107**, 041803 (2011).
75. Chang-Zheng Yuan, Chin. Phys. C **38**, 043001 (2014).
76. M. Ablikim *et al.* [BESIII Collaboration], Phys. Rev. Lett. **114**, 092003 (2015).
77. G. Pakhlova *et al.* [Belle Collaboration], Phys. Rev. D **80**, 091101 (2009).
78. M. Ablikim *et al.* [BESIII Collaboration], Phys. Rev. Lett. **122**, 102002 (2019).
79. G. Pakhlova *et al.* [Belle Collaboration], Phys. Rev. Lett. **100**, 062001 (2008).
80. C. Z. Yuan, P. Wang and X. H. Mo, Phys. Lett. B **634**, 399 (2006).
81. L. Y. Dai, M. Shi, G. Y. Tang and H. Q. Zheng, Phys. Rev. D **92**, 014020 (2015).
82. M. Ablikim *et al.* [BESIII Collaboration], Phys. Rev. D **93**, 011102 (2016).
83. M. Ablikim *et al.* [BESIII Collaboration], Phys. Rev. D **97**, 032008 (2018).
84. M. Ablikim *et al.* [BESIII Collaboration], Phys. Rev. D **96**, 012001 (2017).
85. M. Ablikim *et al.* [BESIII Collaboration], Phys. Rev. D **86**, 071101 (2012).
86. M. Ablikim *et al.* [BESIII Collaboration], Phys. Rev. D **91**, 112005 (2015).
87. X. L. Wang *et al.* [Belle Collaboration], Phys. Rev. D **87**, 051101 (2013).
88. M. Ablikim *et al.* [BESIII Collaboration], Phys. Rev. D **94**, 032009 (2016).
89. X. Y. Gao, C. P. Shen and C. Z. Yuan, Phys. Rev. D **95**, 92007 (2017).
90. J. Zhang, L. Yuan and R. Wang, arXiv:1805.03565 [hep-ph]; J. Zhang and L. Yuan, Int. J. Mod. Phys. A **33**, 1850020 (2018); J. Zhang and L. Yuan, Eur. Phys. J. C **77**, 727 (2017); J. Zhang and L. Yuan, Mod. Phys. Lett. A **32**, 1750184 (2017).
91. Y. Chen, W. F. Chiu, M. Gong, L. C. Gui and Z. Liu, Chin. Phys. C **40**, 081002 (2016).
92. T. V. Uglov, Y. S. Kalashnikova, A. V. Nefediev, G. V. Pakhlova and P. N. Pakhlov, JETP Lett. **105**, 1 (2017).
93. M. Ablikim *et al.* [BESIII Collaboration], Phys. Rev. Lett. **115**, 011803 (2015).
94. V. Bhardwaj *et al.* [Belle Collaboration], Phys. Rev. Lett. **111**, 032001 (2013).
95. E. Eichten, K. Gottfried, T. Kinoshita, K. D. Lane and T. M. Yan, Phys. Rev. D **17**, 3090 (1978) [Phys. Rev. D **21**, 313 (1980)].
96. T. Barnes, S. Godfrey and E. S. Swanson, Phys. Rev. D **72**, 054026 (2005).
97. S. Godfrey and N. Isgur, Phys. Rev. D **32**, 189 (1985); W. Kwong, J. L. Rosner and C. Quigg, Ann. Rev. Nucl. Part. Sci. **37**, 325 (1987); D. Ebert, R. N. Faustov and V. O. Galkin, Phys. Rev. D **67**, 014027 (2003); E. J. Eichten, K. Lane and C. Quigg, Phys. Rev. D **69**, 094019 (2004); B. Q. Li and K. T. Chao, Phys. Rev. D **79**, 094004 (2009); M. Blank and A. Krassnigg, Phys. Rev. D **84**, 096014 (2011).
98. C. F. Qiao, F. Yuan and K. T. Chao, Phys. Rev. D **55**, 4001 (1997).
99. T. Aaltonen *et al.* [CDF Collaboration], Phys. Rev. Lett. **102**, 242002 (2009).
100. T. Aaltonen *et al.* [CDF Collaboration], Mod. Phys. Lett. A **32**, 1750139 (2017).
101. K. YI, Int. J. Mod. Phys. A **28**, 1330020 (2013).
102. M. Ablikim *et al.* [BESIII Collaboration], Phys. Rev. D **91**, 032002 (2015).
103. R. Aaij *et al.* [LHCb Collaboration], Phys. Rev. Lett. **118**, 022003 (2017).
104. Chang-Zheng Yuan, Front. Phys. **10**, 101401 (2015).
105. G. Pakhlova *et al.* [Belle Collaboration], Phys. Rev. Lett. **101**, 172001 (2008).
106. Z. G. Zhao, talk at the “International Workshop on Physics at Future High Intensity

Collider “2-7 GeV in China”, January 13-16, 2015, University of Chinese Academy of Sciences (UCAS), Hefei, China.

107. Eugeny Levichev, talk at “The 9th International Workshop on Charm Physics”, May 21 to 25, 2018, Novosibirsk, Russia.
<https://indico.inp.nsk.su/event/10/session/1/contribution/65/material/slides/0.pdf>